Materials Today Bio 25 (2024) 100975

Contents lists available at ScienceDirect

Materials Today Bio

journal homepage: www.journals.elsevier.com/materials-today-bio

Acellular embryoid body and hydroxybutyl chitosan composite hydrogels promote M2 macrophage polarization and accelerate diabetic cutaneous wound healing

Yue Zhang [a,b,1], Zheng-Hong Chen [c,1], Kun Zhao [d], Yu-Dong Mu [e], Kun-Long Li [d], Zhi-Min Yuan [e], Zhi-Gang Liu [d], Le Han [d], Wei-Dong Lü [d,*]

[a] Department of Pathophysiology, Northwestern University School of Life Sciences, Northwest University, Xi'an, Shaanxi, 710069, China
[b] Key Laboratory of Resource Biology and Biotechnology in Western China, Ministry of Education, Northwest University, Xi'an, Shaanxi, 710069, China
[c] Oncology Department of Integrated Chinese and Western Medicine, Tumor Hospital of Shaanxi Province, Affiliated to the Medical College of Xi'an Jiaotong University, Xi'an, Shaanxi, 710061, China
[d] Department of Thoracic Surgery, Tumor Hospital of Shaanxi Province, Affiliated to the Medical College of Xi'an Jiaotong University, Xi'an, Shaanxi, 710061, China
[e] Department of Clinical Laboratory, Tumor Hospital of Shaanxi Province, Affiliated to the Medical College of Xi'an Jiaotong University, Xi'an, Shaanxi, 710061, China

ARTICLE INFO

Keywords:
Acellular embryoid bodies
Hydroxybutyl chitosan
Diabetic wound healing
Macrophage polarization
Composite hydrogels

ABSTRACT

Diabetic wound healing is delayed due to persistent inflammation, and macrophage-immunomodulating biomaterials can control the inflammatory phase and shorten the healing time. In this study, acellular embryoid bodies (aEBs) were prepared and mixed with thermosensitive hydroxybutyl chitosan (HBC) hydrogels to produce aEB/HBC composite hydrogels. The aEB/HBC composite hydrogels exhibited reversible temperature-sensitive phase transition behavior and a hybrid porous network. *In vitro* analysis showed that the aEB/HBC composite hydrogels exhibited better antimicrobial activity than the PBS control, aEBs or HBC hydrogels and promoted M0 to M2 polarization but not M1 to M2 macrophage repolarization in culture. The *in vivo* results showed that the aEB/HBC composite hydrogels accelerated cutaneous wound closure, re-epithelialization, ingrowth of new blood vessels, and collagen deposition and reduced the scar width during wound healing in diabetic mice over time. Macrophage phenotype analysis showed that the aEB/HBC composite hydrogels induce M2 macrophage reactions continually, upregulate M2-related mRNA and protein expression and downregulate M1-related mRNA and protein expression. Therefore, the aEB/HBC composite hydrogels have excellent antimicrobial activity, promote M2 macrophage polarization and accelerate the functional and structural healing of diabetic cutaneous wounds.

1. Introduction

Wound healing in patients with diabetes, aging, obesity or vascular insufficiency is delayed, resulting in chronic wounds, which are a major public health issues [1–3]. The natural wound healing process consists of three dynamically overlapping phases: inflammation, proliferation, and remodeling. Chronic wound healing is characterized by persistent inflammatory reactions that inhibit proliferation and remodeling [2,4,5]. Macrophages are key regulators of the wound healing process. Macrophages can exhibit different phenotypes due to different stimuli and play a central role in promoting inflammation or regeneration [6,7]. There are two sources of macrophages in tissues: the self-renewal of tissue resident macrophages and the migration and differentiation of bone marrow-derived monocytes from the blood circulation to tissues

Abbreviations: ESCs, embryonic stem cells; EBs, embryoid bodies; ECM, extracellular matrix; HBC, hydroxybutyl chitosan; DMEM, Dulbecco's modified Eagle's medium; SDS, sodium dodecyl sulfate; PBS, phosphate-buffered saline; H&E, hematoxylin and eosin; GAGs, glycosaminoglycans; MAGS, macrophage growth supplement; LB, Luria–Bertani; LPS, lipopolysaccharide; IFN-γ, interferon γ; FDA, fluorescein diacetate; PI, propidium iodide; qRT–PCR, quantitative real-time polymerase chain reaction; ARG1, arginase-1; M-CSF, macrophage colony stimulating factor.

* Corresponding author. Department of Thoracic Surgery, Tumor Hospital of Shaanxi Province, Affiliated to the Medical College of Xi'an Jiaotong University, 309 Yanta West Road, Xi'an, Shaanxi, 710061, China.
E-mail address: wdlu76@aliyun.com (W.-D. Lü).
[1] These authors contributed equally to this work.

https://doi.org/10.1016/j.mtbio.2024.100975
Received 23 October 2023; Received in revised form 31 December 2023; Accepted 22 January 2024
Available online 26 January 2024

[8]. Activated macrophages are divided into M1 macrophages (classically activated macrophages) and M2 macrophages (alternatively activated macrophages) [9]. Both types of macrophages are involved in inflammatory responses, and M1 macrophages exert proinflammatory effects, while M2 macrophages exert anti-inflammatory effects and support wound healing [10]. The transition of pro-inflammatory (M1) macrophages into anti-inflammatory (M2) phenotypes in wounds is impaired in chronic wounds. As macrophages play a key role in the persistence of chronic wound inflammation, immunomodulation is a crucial aspect of treating chronic wounds. Macrophage polarization can be induced by the extracellular environment. Increasing M2 macrophage activation and M2 macrophage-associated cytokine expression in the inflammatory environment is an effective method for wound healing [11–14].

A variety of medical wound dressings are available today as temporary coverings for wounds. Ideal wound dressings should have good histocompatibility, biological safety, adequate physical-mechanical strength, appropriate microstructure and biochemical properties, a moist wound microenvironment, and easy removal from tissue [15]. A single dressing has limitations that cannot meet all of these needs due to the complexity and dynamism of wound repair [16]. Materials for wound dressings include film dressings, foam dressings, alginate dressings, hydrogel dressings and hydrocolloid dressings. Biomaterials, especially macrophage-immunomodulating biomaterials, have been successfully used to control the inflammatory phase and shorten the healing time [17–24]. Embryonic stem cells (ESCs) can be isolated from early embryos or primordial gonads and show unlimited proliferation and multidirectional differentiation *in vitro* [25]. These cells can be induced to generate embryoid bodies (EBs) in serum-free medium. As an embryo-like tissue, EBs can form extracellular matrix (ECM) skeletons [26]. In tissue engineering research on biomaterials from natural sources, acellular technology is widely used to remove the cellular components of tissues or organs while retaining the ECM [27–29]. Due to their off-the-shelf applications, mouse or human EBs have been decellularized and successfully used as scaffold materials in tissue engineering research [30–33]. Although ESC-derived acellular EBs (aEBs) have been proven to promote tissue regeneration, their effects on wound healing need to be further clarified. Moreover, aEBs cannot tightly couple with the surface of wounds during healing due to their loose surface textures.

Hydrogels are one of the best candidates for wound healing and have the advantages of moisturization, bioactive factor release and antimicrobial activity [34–36]. Hydrogels formed in situ can adapt to uneven wound beds and be used as a minimally invasive regeneration system [37]. Thermosensitive hydroxybutyl chitosan (HBC) hydrogels can spontaneously form gels at body temperature without any additional driving factors or chemical reactions [38–40]. HBC hydrogels can generate a durable barrier between the wound and the outside world but have mild cytotoxicity to fibroblasts and vascular endothelial cells [41]. HBC-based composite hydrogels have been extensively used to promote wound healing [42–45].

In this study, aEBs were prepared and mixed with thermosensitive HBC hydrogels, and the *in vitro* antimicrobial activity and effect of the aEB/HBC composite hydrogels on M0 and M1 macrophage polarization were evaluated. Moreover, the *in vivo* effect of aEB/HBC composite hydrogels on mouse diabetic wound healing and macrophage polarization around the wound site were investigated. We hypothesized that the aEB/HBC composite hydrogels could exhibit better *in vitro* antimicrobial activity and *in vivo* wound healing performance than the blank control or aEBs or HBC alone and present different *in vitro* and *in vivo* macrophage polarization.

2. Materials and methods

2.1. Acquisition of aEBs

The mouse ESC line D3 was purchased from the Shanghai Cell Bank of the Chinese Academy of Sciences. The resuscitated cells were cultured in a mouse stem cell serum-free feeder layer-free culture system (Millipore, Billerica, MA, USA). After 20–30 passages, ESCs were isolated from gelatin-coated Petri dishes with Accutase cell separation solution, and the cell density was adjusted to 4×10^6 cells/mL for further use. Dynamic suspension culture was carried out in Dulbecco's modified Eagle's medium (DMEM) containing 15 % calf serum, 1 % penicillin–streptomycin, 2 mM L-glutamine and 0.1 mM β-mercaptoethanol at 37 °C and 5 % CO_2 with rotation at 40 rpm for 3 days, and EBs were collected by gravity sedimentation [46]. The EBs were decellularized with 0.5 % w/v sodium dodecyl sulfate (SDS) at 37 °C for 24 h, treated with phosphate-buffered saline (PBS) containing 20 U/mL DNase I and 0.2 mg/mL RNase A at 37 °C for 24 h, and finally rinsed with a large amount of sterile PBS. aEBs were suspended in sterile PBS (approximately 1×10^4/mL) with 5 % penicillin–streptomycin and stored at 4 °C for further use.

2.2. Histological evaluation of aEBs

Tissue samples were fixed with 4 % formaldehyde for paraffin sectioning. Routine hematoxylin and eosin (H&E) staining was used to detect the degree of cellular removal. After the EBs and aEBs were freeze-dried, DNA was extracted, and the DNA content before and after decellularization ($n = 10$) was determined with the PicoGreen dsDNA quantitative detection kit (Invitrogen, Thermo Fisher Scientific, Carlsbad, CA, USA) [47]. Collagen fibers were stained by the Masson's trichrome method, and glycosaminoglycans (GAGs) were examined by Scott's Alcian blue staining. Collagen I, collagen IV, fibronectin and laminin components were examined by immunofluorescence staining with rabbit anti-collagen I monoclonal antibodies (1:200, Abcam, Cambridge, UK), rabbit anti-collagen IV monoclonal antibodies (1:100, Abcam), rabbit anti-fibronectin monoclonal antibodies (1:100, Abcam), and rabbit *anti*-laminin polyclonal antibodies (1:50, Abcam). Alexa Fluor 488-labeled goat anti-rabbit IgG (1:1000, Abcam) was used as the secondary antibody, and cell nuclei were stained with DAPI. The immunofluorescence staining procedure was previously described [48].

2.3. aEBs mixed with HBC hydrogel

Commercial thermosensitive HBC hydrogels (Horizon International Medical Equipment Co., Ltd., Beijing, China) were stored at 4 °C for later use. HBC hydrogel preparation was previously described [41]. In brief, 10 g chitosan was alkalinized at 15 °C by 100 mL KOH (50 %, w/w) with N2. The chitosan was dispersed in 200 mL isopropanol/water (8:1) and mixed with 200 mL 1,2-butene oxide in an autoclave after additional KOH solution was removed. The excess alkylating agent was removed via nitrogen bubbling after 96 h of reaction time at room temperature. The filtrate was then reduced in a rotary evaporator following pressure filtration to remove any unreacted components. In the end, the precipitation was gathered on a glass sintering suction filter, extensively rinsed with 8–10 times its volume of acetone, and dried at 50 °C in a vacuum drying cupboard. The 2 % HBC solution was then prepared and stored at 4 °C until used. When the temperature was higher than 24 °C, the HBC became hydrogels. aEBs and thermosensitive HBC hydrogels were mixed at 4 °C (vol/vol 1:2) for further use. The aEB/HBC composite hydrogels were lyophilized for 24 h, and the ultrastructure was examined with a Hitachi S4800 scanning electron microscope (Hitachi, Tokyo, Japan); aEBs and HBC hydrogels were used as controls.

2.4. Antimicrobial activity evaluation

The *in vitro* antibacterial activity of the aEB/HBC composite hydrogels was evaluated by inoculating with *Staphylococcus aureus* (*S. aureus*, a gram-positive bacteria) and *Escherichia coli* (*E. coli*, a gram-negative bacteria) respectively; PBS, aEBs and HBC hydrogels were used as controls. Samples of aEBs, HBC hydrogels and aEB/HBC composite

hydrogels were sterilized by irradiation with ultraviolet light for 48 h. The bacteria were inoculated in sterilized broth for 24 h at 37 °C and 200 rpm in a shaking incubator and diluted with fresh Luria–Bertani (LB) broth to a concentration of 1×10^6 CFU/mL for further use. Subsequently, 1 mL of PBS, aEB, HBC hydrogel or aEB/HBC composite hydrogel was mixed with 1 mL of diluted bacteria in a sterile 2-mL EP tube and incubated at 37 °C and 200 rpm for 12 h. Finally, the solution was removed and diluted 1×10^4 times, and 20 μL of the diluted solution was inoculated on LB agar plates and cultured for 18 h. The bacterial clone number was counted, and the bacterial survival rate was calculated using the following equation:

$$\text{Bacterial survival rate (R \%)} = 100 \times C_x/C_0 \,\% \quad (1)$$

Where C_0 represents the clone number of the PBS control solutions and C_x represents the clone number of aEBs, HBC hydrogels or aEB/HBC composite hydrogels. All measurements were performed in triplicate.

2.5. In vitro macrophage induction and immunophenotype detection

2.5.1. Macrophage culture and induction

Mouse bone marrow-derived macrophages (M0) were purchased from ScienCell (m1920). After resuscitation, macrophages were cultured on sterile 6-well plates in macrophage culture medium (ScienCell, m1921) containing 1 % macrophage growth supplement (MAGS), 5 % fetal bovine serum and 1 % penicillin–streptomycin at 37 °C and 5 % CO_2 for 3 days. The cell concentration was adjusted to 1.5×10^5 cells/mL in macrophage culture medium for further induction. The aEB/HBC composite hydrogels (100 μL) were added to the above M0 macrophages containing culture medium (1 mL), with PBS, aEBs and HBC hydrogels used as controls. The incubation lasted for 24 h for further testing. For analysis of the influence of the aEB/HBC composite hydrogels on M1-to-M2 polarization, M0 macrophages were induced to M1 macrophages with 100 ng/mL lipopolysaccharide (LPS) from *E. coli* (Sigma-Aldrich, St. Louis, MO, USA) and 20 ng/mL mouse interferon γ (IFN-γ, Sigma-Aldrich) as described by Anders and colleagues [49]. PBS, aEBs, HBC hydrogels and aEB/HBC composite hydrogels (100 μL) were added to the above M1 macrophage-containing culture medium (1 mL) and incubated at 37 °C and 5 % CO_2 for 24 h for further investigation.

2.5.2. Cell growth analysis

Light microscopy examinations were performed by fluorescein diacetate (FDA) and propidium iodide (PI) staining for live and dead cells ($n = 8$) as previously described [47]. The macrophage numbers ($n = 8$) were detected with the alamarBlue assay [50]. The Supplementary file 1 presents the cell proliferation assay conducted on L929 mouse fibroblast cells.

2.5.3. Immunofluorescence staining for macrophage polarization

Immunofluorescence staining was performed to identify macrophages and their subtypes. Total macrophages were stained with rat *anti*-F4/80 monoclonal antibodies (1:50, Invitrogen). M1 and M2 macrophages were stained with rat anti-CD86 and anti-CD206 monoclonal antibodies (1:200, Invitrogen), respectively. Alexa Fluor 555-labeled donkey anti-rat IgG (1:1000, Abcam) was used as the secondary antibody, and cell nuclei were stained with DAPI. The immunofluorescence staining procedure was previously described [48,51].

2.5.4. Quantitative real-time polymerase chain reaction (qRT–PCR)

RNA was isolated using TRIzol reagent (Invitrogen). The PCR primers for TNF-α, arginase-1 (ARG1) and GAPDH were previously described [51]. PCR was conducted with a LightCycler 96 System (Roche, Basel, Switzerland). The gene expression levels of TNF-α and ARG1 were normalized to that of GAPDH ($n = 8$). Macrophage polarization was quantified by determining the ARG1/TNF-α gene expression ratio [52].

2.5.5. Cytokine detection with enzyme-linked immunosorbent assays (ELISAs)

The cell culture supernatants were collected, and TNF-α and TGF-β levels in the supernatants ($n = 8$) were assayed with an ELISA kit (R&D Systems, Minneapolis, MN, USA) according to the manufacturer's protocol.

2.6. Effect of the aEB/HBC composite hydrogels on healing of diabetic cutaneous wounds

2.6.1. Animals

The protocols and procedures for animal experiments were approved by the Animal Care and Use Committee of Xi'an Jiaotong University (No. XJTUAE2023-1376). Healthy 8-week-old male BALB/c mice without specific pathogens (body mass approximately 20 g) were intraperitoneally injected with 10 mg/mL streptozotocin (50 mg/kg) once per day for 5 days [53]. During this period, the blood glucose level was monitored at 9:00 a.m. If the blood glucose level was higher than 16 mmol/L, the diabetic mice were successfully established. The mice were fed high-fat and high-sugar feed for another 2 weeks before the wound was created.

2.6.2. Induction of cutaneous wounds and treatment protocol

The mice were anesthetized by an intraperitoneal injection of 50 mg/kg pentobarbital sodium (concentration 10 mg/mL), and then, the back surface hair was shaved. Immediately after the sterile full-thickness skin defect wound was produced with a 6-mm diameter punch, the wound was covered with 200 μL of PBS or 200 μL of aEBs (concentration 1×10^4/mL), HBC hydrogel or aEB/HBC composite hydrogel ($n = 18$) in the liquid state (4 °C). The wound was bound with a sterile bandage. The wound was treated in the same way every two days unless the wound was closed. Six mice in each group at different time points were used. At 0 (immediate), 3, 7 and 14 days after injury, the wound healing area was imaged with a camera, and the unhealed area of the wound was evaluated with ImageJ 1.52a image analysis software (NIH, Bethesda, MD, USA). The wound healing rate was calculated using the following equation:

$$\text{Wound healing rate (\%)} = 100 \times (A_0\text{-}A_u)/A_0 \quad (2)$$

Where A_u represents the unhealed area of the wound and A_0 represents the related original wound area. At different time points after injury, the mice ($n = 6$) were killed by decapitation after being anesthetized. Skin tissue 5 mm around the wound surface and wound margin was collected and divided into two parts. One part of the wound tissue was fixed in 4 % paraformaldehyde for paraffin sectioning. The other part of the wound tissue was frozen for further analysis.

2.6.3. Histological and immunohistochemical/immunofluorescence staining for wound healing

Paraffin sections were stained with H&E and Masson's trichrome to investigate wound healing. Re-epithelialization, granulation tissue width and collagen area were quantified with ImageJ [54]. Collagen I and collagen III monoclonal antibodies (1:100, Abcam) were used to investigate mature type I and newly formed type III collagens. The immunohistochemical staining procedures were previously described [55]. CD31 monoclonal antibodies (1:100, Abcam) and α-SMA monoclonal antibodies (1:200, Abcam) for double immunofluorescence staining were used to detect microvessels [48,56]. Alexa Fluor 555-labeled donkey anti-rat IgG (1:1000, Abcam) and Alexa Fluor 488-labeled goat anti-rabbit IgG (1:1000, Abcam) were used as secondary antibodies. Cell nuclei were stained with DAPI.

2.6.4. Macrophage polarization evaluation for wound healing

Immunofluorescence staining was performed to identify macrophages and their subtypes. Rat *anti*-F4/80 monoclonal antibodies (1:50,

Invitrogen) were used to stain total macrophages. Dual staining of the macrophage M1/M2 subtypes was conducted with rat anti-mouse CD86 monoclonal antibodies (1:200, Invitrogen) and rabbit anti-mouse CD206 antibodies (1:500, Abcam). RNA was isolated from the harvested skin tissues surrounding the wound site using TRIzol reagent (Invitrogen). Macrophage polarization in the tissues was also quantified by determining the ARG1/TNF-α gene expression ratio as in the cell culture. For western blot analysis, tissues around the wound site were harvested, weighed, and sliced into pieces. Proteins were extracted and assayed and then separated by SDS–PAGE as previously described [51]. The protein bands ($n = 6$) for TNF-α, ARG1, and β-actin were scanned and quantified with ImageJ software. Protein expression values were normalized to the β-actin levels.

2.7. Statistical analysis

The results are presented as the mean ± standard deviation (SD). Statistical analyses were performed using IBM SPSS Statistics (version 26.0, IBM Corp., Armonk, NY, USA). Statistical comparisons were performed with one-way analysis of variance (ANOVA) followed by Tukey's multiple comparisons test. The Kruskal–Wallis test and pairwise Dunn's multiple comparisons test were used to compare cytokine levels of macrophage culture. A value of $p < 0.05$ was considered statistically significant.

3. Results and discussion

The delayed healing of diabetic wounds can be attributed to the presence of persistent inflammation. However, the utilization of macrophage-immunomodulating biomaterials has demonstrated the ability to regulate the inflammatory phase, resulting in a reduction of healing time [18,19,22]. In the present study, aEBs were prepared and combined with thermosensitive HBC hydrogels to fabricate a biomaterial with macrophage-immunomodulating properties, intended for the purpose of promoting diabetic wound healing.

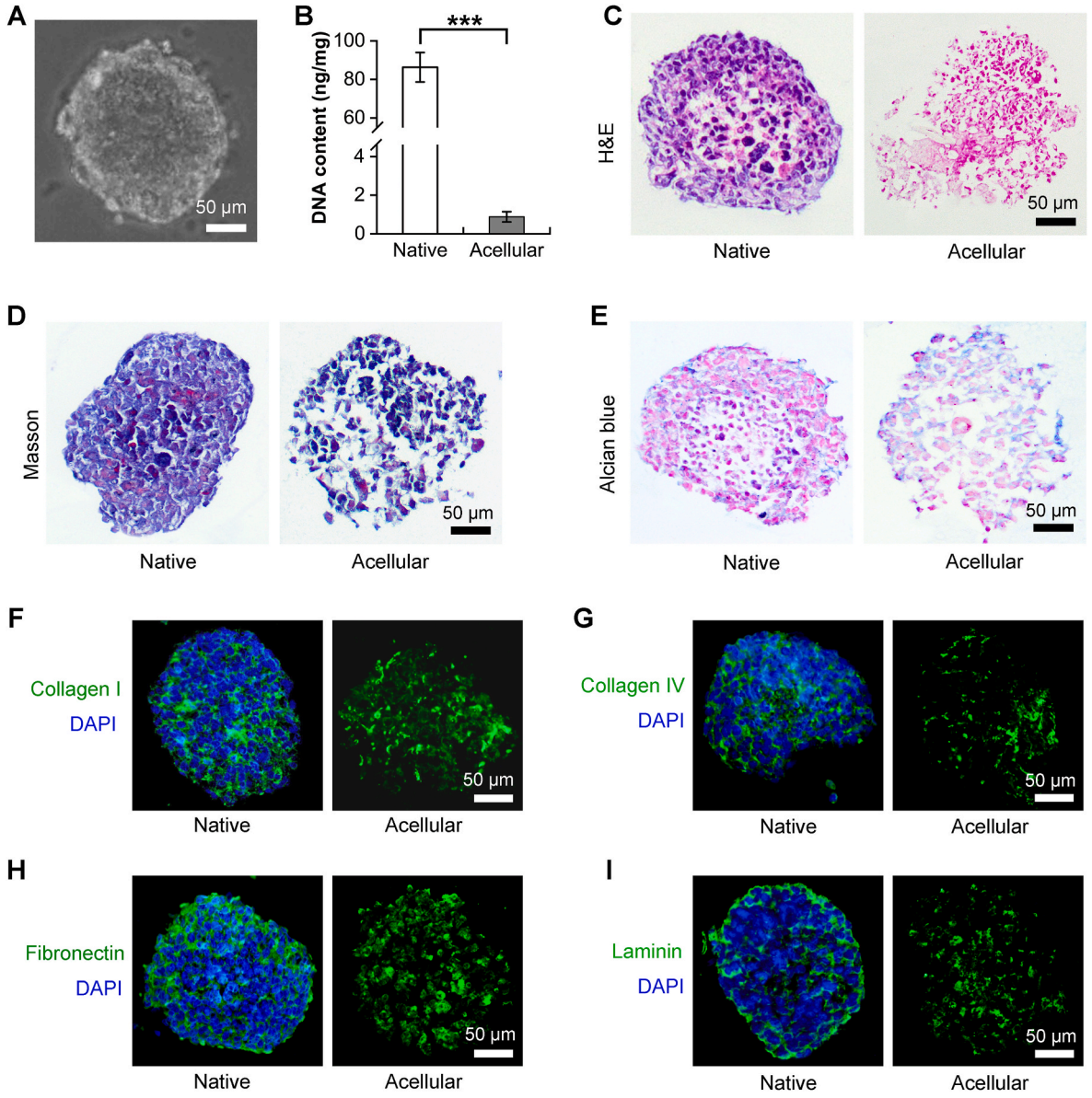

Fig. 1. Representative histological properties of native and aEBs. (A) Native EB under a light microscope. (B) Comparison of the DNA content of EBs before and after cell removal ($n = 10$, $^{***}p < 0.001$). (C–E) H&E staining showing cellular removal, Masson staining showing collagen fibers and Scott's Alcian blue staining showing GAGs in native and aEBs. (F–I) Collagen I, collagen IV, fibronectin and laminin immunofluorescence analysis of native and aEBs.

3.1. Successful preparation of aEBs

Fig. 1 shows that the cellular structures of the aEBs were completely removed, and the components of the ECM were unchanged compared with those of the native EBs. Fig. 1A shows light microscopy images of EBs, which had a diameter of approximately 200 μm. Fig. 1B shows that the DNA content of aEBs was significantly lower than that of native EBs (0.77 versus 86.91 ng/mg, $p < 0.001$). Cellular removal shown by H&E staining, collagen fibers shown by Masson staining and GAGs shown by Scott's Alcian blue indicated that the cellular components of the aEBs were completely removed, while collagen and GAGs were basically retained (Fig. 1C–E). Collagen I, collagen IV, fibronectin and laminin immunofluorescence staining (Fig. 1F–I) indicated that collagen I and fibronectin were well preserved after cell removal. However, collagen IV and laminin, which are the main components of the basement membrane, became dispersed. In this study, we used mouse ESCs to produce EBs, used SDS to decellularize the EBs, and obtained ECM scaffolds with radical cellular removal and almost complete preservation of the ECM composition and structure. The maintenance of ECM structural proteins, GAGs and bound matrix-associated growth factors is important in tissue regeneration [57,58]. This finding shows that the aEB scaffold is suitable as a tissue engineering material and is worthy of further study and use.

3.2. Preparation of aEB/HBC composite hydrogels

Fig. 2A shows the preparation procedure of the aEB/HBC composite hydrogels. aEBs and HBC composite hydrogels were mixed at 4 °C to produce the aEB/HBC composite hydrogels. Fig. 2B shows that aEBs were kept in the solution state from 4 to 37 °C. HBC and the aEB/HBC composite showed reversible temperature-sensitive phase transition behavior, maintaining the solution state at low temperatures (4 °C) and converting to hydrogels at elevated temperatures (higher than 25 °C). SEM examination showed porous surfaces for aEBs, connected porous networks for HBC hydrogels, and aEBs embedded in the connected porous structure of HBC hydrogels for aEB/HBC composite hydrogels (Fig. 2C). Thermosensitive HBC hydrogels remained in a liquid state at low temperature to permit the loading of biological components for wound healing [42]. The aEB/HBC composite hydrogels have the advantages of thermosensitive hydrogels and ESC-derived ECM composition and structure. However, the aEB/HBC composite hydrogels have limitations including potential local cytotoxicity and stability over time.

3.3. The aEB/HBC composite hydrogels show in vitro antimicrobial activity

The aEB/HBC composite hydrogels exhibited excellent antibacterial activity. As shown in Fig. 3A and B, the aEB group exhibited *S. aureus* viability similar to that of the PBS control group (97.85 % versus 100 %, $p = 0.769$), and the HBC group had fewer *S. aureus* colonies than the PBS control group (2.82 % versus 100 %, $p < 0.001$). The aEB/HBC group had the fewest *S. aureus* colonies (1.34 % versus 2.82 % compared with the HBC group, $p = 0.003$) among the four groups. Fig. 3A and C shows that the aEB group had fewer *E. coli* colonies than the PBS control group (86.59 % versus 100 %, $p = 0.043$), and the aEB/HBC group had fewer *E. coli* colonies than the HBC group (2.96 % versus 5.01 %, $p = 0.009$). The HBC group showed fewer *E. coli* colonies than the aEB group ($p < 0.001$). In chronic wounds such as in diabetes, damage to the physiological structure of the skin promotes the colonization of pathogens [59]. Smart hydrogels or coacervates can be used as wound dressings to prevent bacterial colonization at the wound site [60–63]. The HBC hydrogels had excellent antibacterial properties due to the high content of chitosan. The aEB/HBC group exhibited better antibacterial properties than the HBC group, which could be due to the hydrogel components and antibiotic residues during preparation and preservation.

3.4. The aEB/HBC composite hydrogels induce different macrophage polarization for M0 and M1 macrophages in culture

M0 naive macrophages are induced and differentiated from monocytes by macrophage colony stimulating factor (M-CSF) [64]. These cells

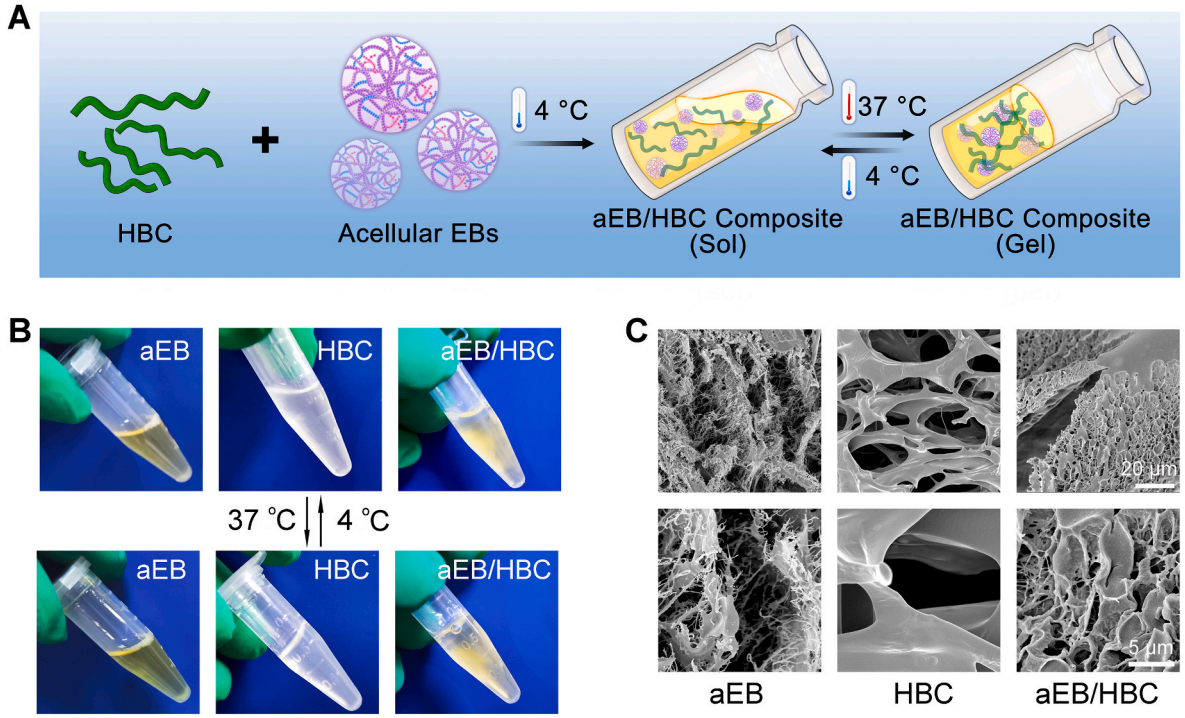

Fig. 2. Preparation procedure and ultrastructural comparisons of aEBs, temperature-sensitive HBC hydrogels and their mixtures. (A) Schematic showing the preparation of the aEB/HBC composite hydrogels. (B) Representative gross appearance of the aEBs, HBC hydrogels and aEB/HBC composite hydrogels at 4 °C and 37 °C. (C) Representative SEM examination of original and amplified images.

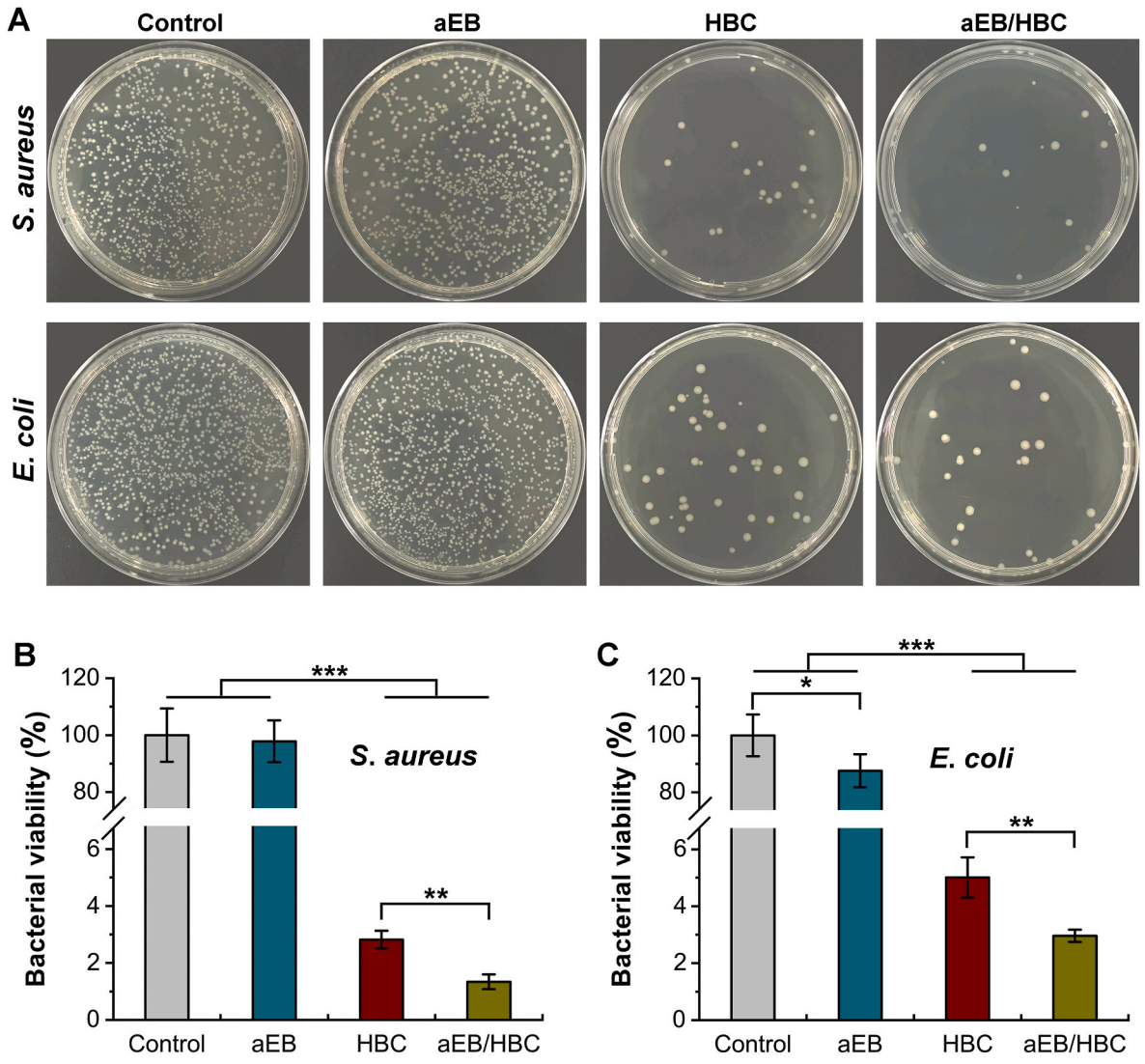

Fig. 3. Antimicrobial activity of the PBS control, aEBs, HBC hydrogels and aEB/HBC composite hydrogels. (A) Representative *S. aureus* and *E. coli* colony formation on LB plates. (B) Quantitative *S. aureus* viability ($n = 3$). (C) Quantitative *E. coli* viability ($n = 3$). *$p < 0.05$, **$p < 0.01$ and ***$p < 0.001$.

are highly plastic and can be induced to polarize M1 macrophages by IFN-γ and LPS. In the present study, the effect of aEB/HBC composite hydrogels on naive M0 and polarized M1 macrophages was investigated.

3.4.1. The aEB/HBC composite hydrogels promote M0 to M2 macrophage polarization

The live/dead cell staining of the M0 macrophages cultured at 24 h, as shown in Fig. 4A, revealed that the HBC group had a similar circular shape to the PBS control group, while the aEB and the aEB/HBC groups presented the most macrophage tentacle-like processes. The aEB group had the fewest red-stained dead cells. Fig. 4B shows that the aEB group had lower cell numbers per well than the control group ($p = 0.003$). The HBC and aEB/HBC groups had equivalent cell numbers to the control group ($p = 0.696$ and 0.152), but the aEB/HBC group had higher cell numbers than the HBC group ($p = 0.014$). HBC hydrogels were reported to be cytotoxic to fibroblasts and vascular endothelial cells [41], but the present results indicated little cytotoxicity to macrophages, as well as to L929 mouse fibroblast cells (Supplementary file 1, Fig. S1). Moreover, the HBC and aEB hybrid hydrogels showed better support of macrophage and fibroblast cell proliferation than the aEBs or the HBC hydrogels.

Fig. 4C shows that most of the cells were F4/80 positive. Fig. 4C and D reveal that the HBC group had the largest number of CD86-positive cells, while the aEB/HBC group had the lowest number. The aEB group had fewer CD86-positive cells than the control group ($p < 0.001$). Fig. 4C and E shows that the aEB/HBC group had the largest number of CD206-positive cells, while the control group had the lowest number. The aEB group had more CD206-positive cells than the HBC group ($p < 0.001$). Fig. 4F reveals that the mRNA ratio of ARG1/TNF-α was lowest in the control group and highest in the aEB/HBC group. The HBC group had a lower ARG1/TNF-α ratio than the aEB group ($p < 0.001$). Cytokine analysis showed that the HBC group expressed the highest TNF-α levels, and the control group expressed the second highest TNF-α levels (Fig. 4G). The aEB group had similar TNF-α expression as the aEB/HBC group ($p = 0.822$). The TGF-β expression shown in Fig. 4H indicates that the lowest expression level was in the control group and the highest expression in the aEB/HBC group. The aEB group had higher TGF-β expression than the HBC group ($p = 0.026$). This finding demonstrated that both aEBs and aEB/HBC composite hydrogels upregulated M2-related cytokine expression and downregulated M1-related cytokine expression.

3.4.2. The aEB/HBC composite hydrogels fail to induce M1 to M2 macrophage polarization

Fig. 5A shows a schematic illustration of the induction of M0 macrophages into M1 macrophages with LPS and IFN-γ, and the M1

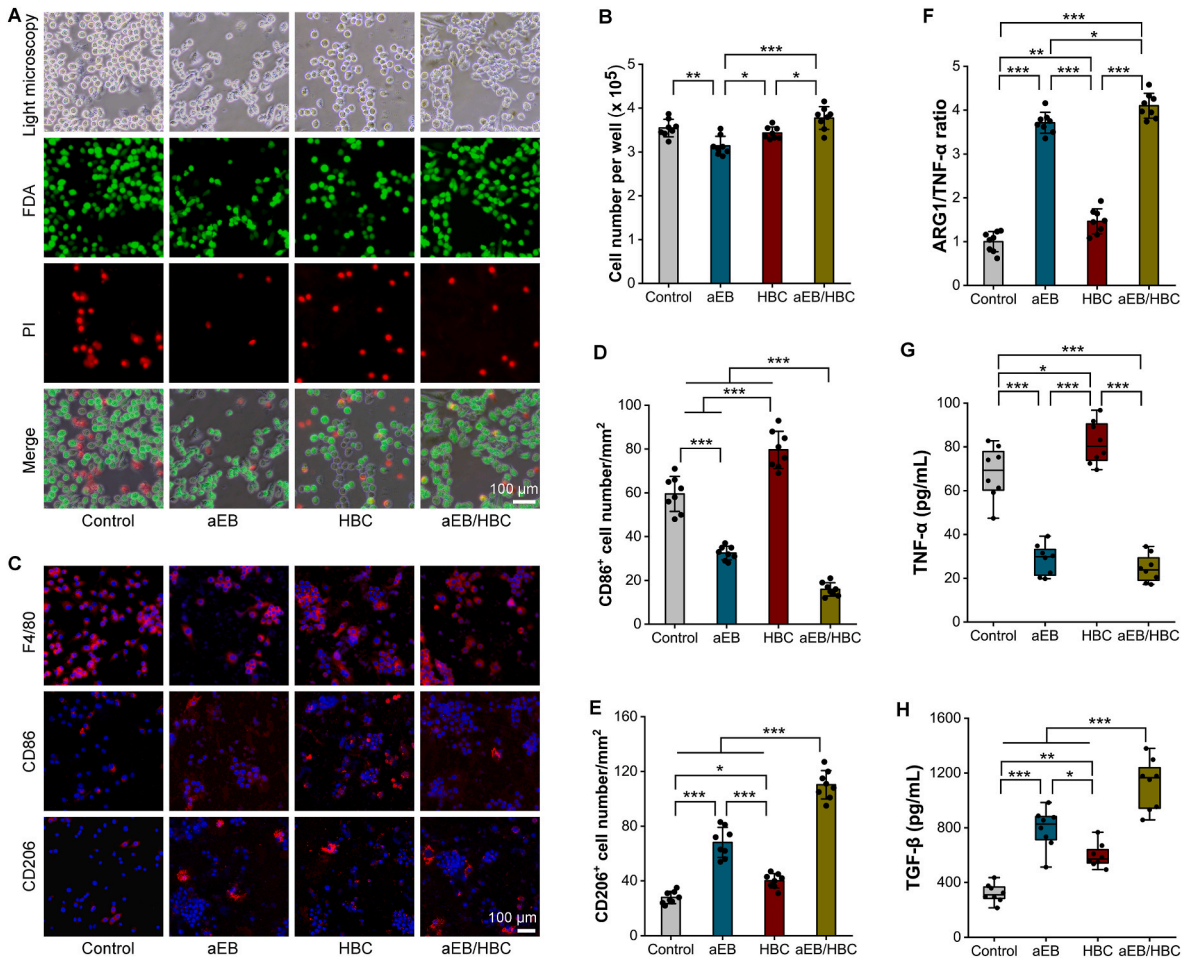

Fig. 4. The *in vitro* polarization of M0 macrophages treated with the PBS control, aEBs, HBC hydrogels and aEB/HBC composite hydrogels. (A) Representative light microscopic examination and FDA-PI staining of live/dead cells at 24 h culture. (B) Live cell number comparisons for the four groups. (C) Representative immunofluorescence images of F4/80+ cells (red, pan macrophage marker), $CD86^+$ cells (red, M1 marker), CD206+ cells (red, M2 marker) and nuclei (DAPI, blue). (D, E) M1 macrophage (D, $CD86^+$) and M2 macrophage (E, CD206+) number comparisons for the four groups. (F) Relative ratios of ARG1 and TNF-α mRNA in the four groups. (G, H) The M1 macrophage-related cytokine TNF-α (G) and the M2 macrophage-related cytokine TGF-β (H) were assayed by ELISAs ($n = 8$). *$p < 0.05$, **$p < 0.01$ and ***$p < 0.001$. (For interpretation of the references to color in this figure legend, the reader is referred to the Web version of this article.)

macrophages were identified by dual positive staining with F4/80 and CD86 (Fig. 5B). Fig. 5C and D shows that the control group, the aEB group and the HBC group had similar numbers of CD86-positive cells, and the aEB/HBC group had the lowest number of CD86-positive cells. Fig. 5C and E shows that the four groups had similar numbers of CD206-positive cells. Fig. 5F shows that the mRNA ratio of ARG1/TNF-α was highest in the aEB/HBC group, and the other three groups had similar ARG1/TNF-α ratios. Fig. 5G shows that the aEB group had similar TNF-α levels to the control group and the aEB/HBC group ($p = 0.504$ and 0.321) but had lower TNF-α levels than the HBC group ($p = 0.027$). The aEB/HBC group had lower TNF-α levels than the control and HBC groups ($p = 0.019$ and $p < 0.001$). Fig. 5H shows that the four groups had similar TGF-β expression levels. The results confirmed that the aEB/HBC composite hydrogels fail to promote M1 to M2 transformation but have an inhibitory effect on M1 macrophages. This finding is consistent with a previous study showing that the formed M1 macrophages attenuated mitochondrial oxidative phosphorylation, lacked plasticity and could not be repolarized to M2 macrophages [65]. As a result, the prohealing M2 macrophages must come from precursor macrophages rather than be reprogrammed from M1 macrophages.

3.5. The aEB/HBC composite hydrogels promote cutaneous wound healing in diabetic mice

Fig. 6A and B shows images of wound healing and the wound healing rate for the wounds treated with the PBS control, aEBs, HBC hydrogels and aEB/HBC composite hydrogels at different time points. The wound area in the four groups decreased with time. On Day 3, the PBS control group and the aEB group had similar wound healing rates, as did the aEB/HBC group and the HBC group. However, the two latter groups had higher wound healing rates than the two former groups ($p < 0.001$). On Days 7 and 14, the PBS control group had the lowest wound healing rate, and the HBC group had a similar wound healing rate as the aEB group ($p = 0.784$ and 0.138). The aEB/HBC group had a similar wound healing rate as the HBC group on Day 7 ($p = 0.273$) and had a higher wound healing rate than the HBC group on Day 14 ($p = 0.031$). The trends in wound healing rate decreased over time for the four groups, especially for the control group. These results demonstrated that aEBs or HBC hydrogels accelerated wound healing in diabetic mice, and the aEB/HBC composite hydrogel exerted the best effect on wound healing. The loose surface textures of aEBs prevent them from tightly adhering to wounds during healing, while the HBC hydrogels form spontaneously at body temperature and generate a durable barrier between the wound and the outside world but have a mild cytotoxic effect. The aEB/HBC composite hydrogels work better than aEB or HBC alone duo to integrating the

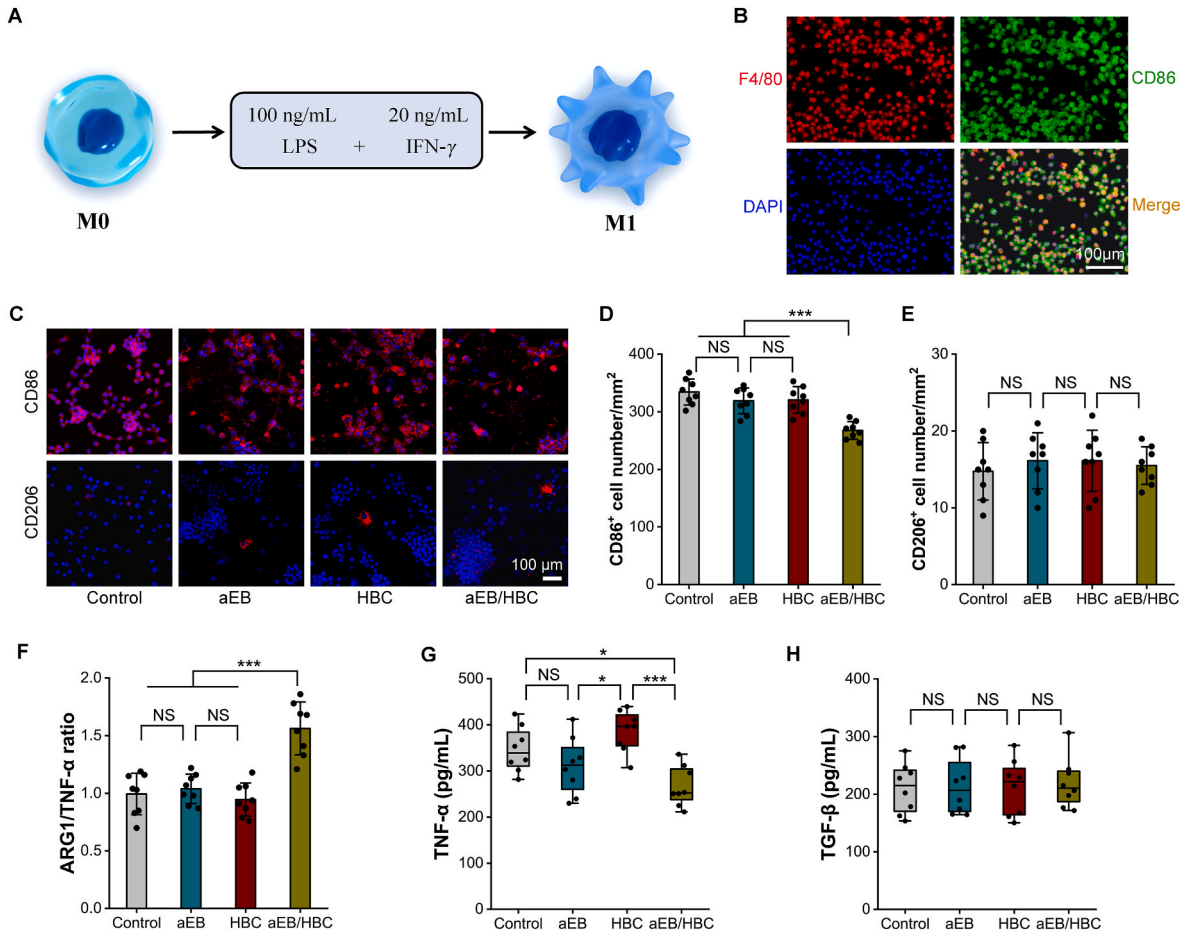

Fig. 5. The *in vitro* phenotypic transformation of M1 macrophages. (A) Schematic illustration of the induction of M0 macrophages into M1 macrophages. (B) M1 macrophages were identified by dual staining with F4/80 and CD86, and nuclei were stained with DAPI. (C) Representative immunofluorescence images of M1 ($CD86^{+}$) and M2 macrophages (CD206+) after M1 macrophages were treated with the PBS control, aEBs, HBC hydrogels and aEB/HBC composite hydrogels. (D, E) M1 (D) and M2 macrophage (E) number comparisons. (F) Relative ARG1 and TNF-α mRNA ratios in the four groups. (G, H) The expression levels of TNF-α (G) and TGF-β (H) were assayed by ELISAs ($n = 8$). $*p < 0.05$, $***p < 0.001$ and NS, no significance.

advantages of both while removing their drawbacks.

Fig. S2 shows H&E and Masson's trichrome staining of normal mouse skin. The normal skin structure includes epidermis, dermis and subcutaneous tissue. The epidermis is thinner and lacks blood vessels, the dermis is thicker and consists of collagen fibers, blood vessels, nerve bundles, lymphatic vessels, and hair follicles, and the subcutaneous tissue is the thickest and includes adipocytes, smooth muscles, and connective tissues. Fig. 6C shows the histological performance of wound healing at different time points. An inflammatory response around the wound was observed on Day 3 in the four groups. The epithelial defects and widths of granulation tissues were decreased, and collagen deposition density increased with time. The epithelial defects were almost closed in the aEB, HBC and aEB/HBC groups on Day 14. Accessory structures in the skin, such as hair follicles and nerves, were observed in the aEB group and the aEB/HBC group, especially in the aEB/HBC group. This finding indicated that aEBs promoted skin structural and functional healing and reduced scar healing, and the aEB/HBC composite hydrogels showed the advantages of aEBs and accelerated wound structural and functional healing.

Wound re-epithelialization of the epidermis (Fig. 6D) and collagen area in the dermis (Fig. 6F) continually increased, and scar width (Fig. 6E) continually decreased from Day 3 to Day 14. Wound re-epithelialization induced by the aEB/HBC composite hydrogels on Day 3 was higher than that in the other groups ($p < 0.001$). On Day 7 and Day 14, the aEB/HBC group had similar re-epithelialization as the HBC group. The scar width in the aEB/HBC group was similar to that in the aEB group but smaller than that in the PBS control group or the HBC group on Day 3 ($p < 0.001$). The aEB/HBC group had the smallest scar width on Days 7 and 14. The PBS control group had the smallest collagen area from Day 3 to Day 14. The aEB/HBC group had a similar collagen area as the HBC group on Day 7 and the largest collagen area on Day 3 and Day 14 compared with the other groups.

Furthermore, the collagen type I and III immunohistochemical staining and relative positive area on Day 14 are shown in Fig. 7A–C. The control group had a collagen type I-positive area comparable to that of normal mouse skin ($p = 0.363$) but presented a lower collagen type I-positive area than the HBC group ($p = 0.004$). The aEB/HBC group had the highest collagen type I-positive area, and the aEB group had the second highest positive area. The normal mouse skin group had the lowest collagen type III-positive area, and the aEB group had the second lowest positive area. The other three groups had similar collagen type III-positive areas.

The ingrowth of new blood vessels accelerates the wound healing process. CD31 and α-SMA double immunofluorescence staining on Day 14 was used to evaluate microvessels. The CD31-positive area represents the newly formed microvessels, and the CD31 and α-SMA double-positive area represents the mature newly formed microvessels. As shown in Fig. 7D and E, the normal mouse skin group had the fewest newly formed microvessels. The aEB, HBC and aEB/HBC groups had similar microvessel numbers. The aEB and the aEB/HBC groups had more microvessels than the control group ($p = 0.021$ and $p < 0.001$). Fig. 7D and F shows that the control group had the lowest proportion of

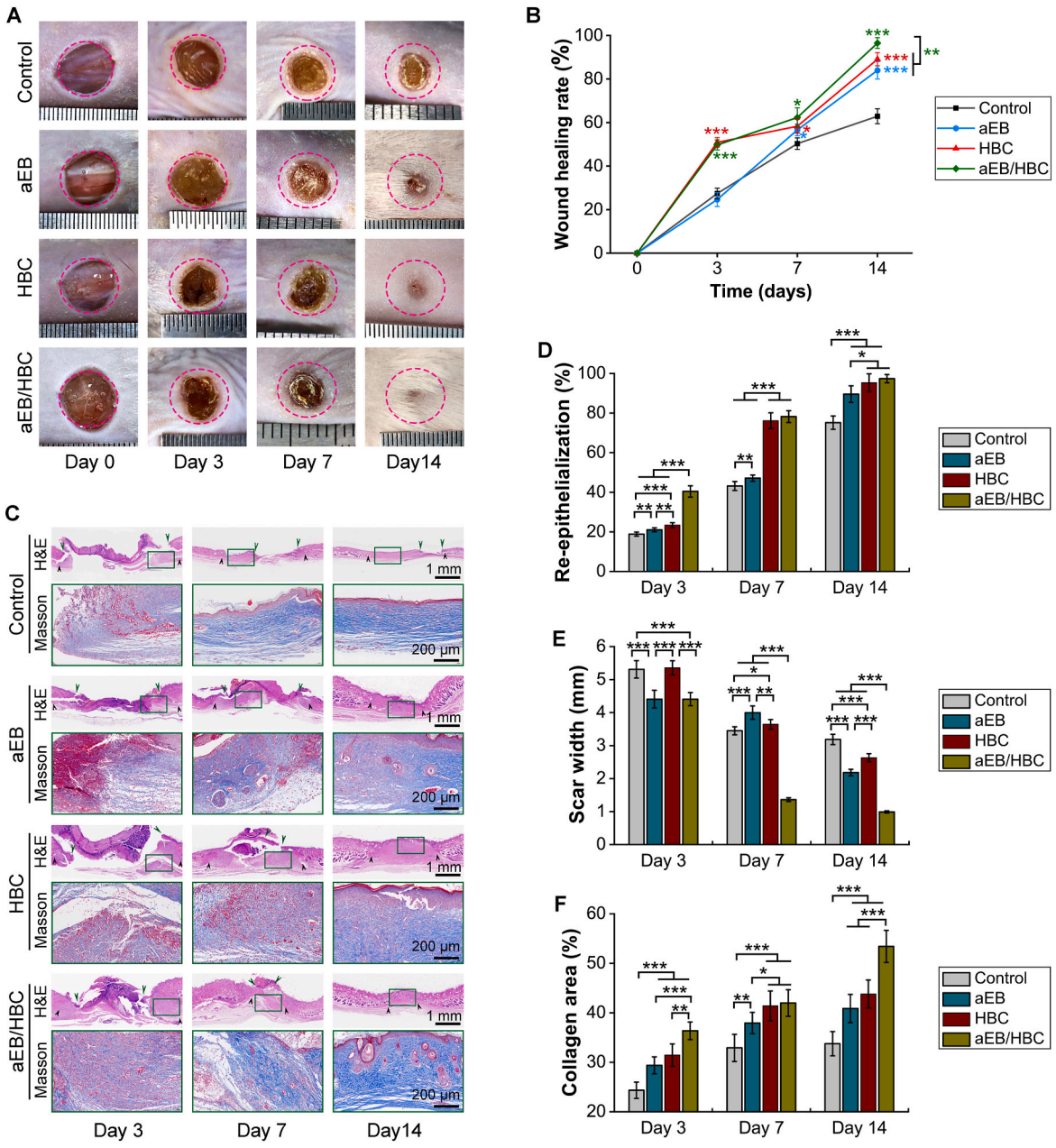

Fig. 6. The gross investigation and histological staining of diabetic wound healing at different times. (A) Representative gross appearance of full-thickness skin wound healing on Days 0, 3, 7 and 14 in the blank control, acellular EB, HBC hydrogel and aEB/HBC composite hydrogel groups. (B) Quantification of the wound healing area in the four groups ($n = 6$). (C) Representative H&E staining and corresponding Masson's trichrome staining in the four groups on Days 3, 7 and 14. (D) Quantification of wound re-epithelialization, as shown by the distance between the green arrows of H&E staining ($n = 6$). (E) Quantification of scar widths, as shown by the distance between the black arrows of H&E staining ($n = 6$). (F) Quantification of mean collagen deposition, as shown by Masson's trichrome staining ($n = 6$). $^{*}p < 0.05$, $^{**}p < 0.01$ and $^{***}p < 0.001$. (For interpretation of the references to color in this figure legend, the reader is referred to the Web version of this article.)

CD31 and α-SMA double-positive newly formed microvessels. The aEB/HBC group had a similar mature microvessel proportion as the normal mouse skin group. These groups both had a larger proportion of mature microvessels than the aEB and HBC groups. Fig. 7G shows that the aEB/HBC group had more microvessels with larger diameters, suggesting the maturation of blood vessels in the aEB/HBC composite hydrogel group over time.

Wounds do not heal in nonbleeding tissues, and tissue ischemia is the main obstacle to wound healing [66]. The wound healing process can be accelerated by treatment or delayed by factors such as diabetic, venous, and pressure ulcers [67,68]. The increase in new microvessel growth accelerates the wound healing process. In the present study, the aEB/HBC composite hydrogel group had accelerated mature newly formed microvessels, which promoted the wound healing process.

3.6. The aEB/HBC composite hydrogels promote in vivo M2 macrophage polarization

Fig. S3 shows the F4/80 immunofluorescence staining for mouse normal skin and wound skin on Day 3. F4/80-positive total macrophages were present in the dermis and subcutaneous tissue of mouse normal skin and abundantly enriched at the junction of wounds and normal tissues. Immunofluorescence dual staining of CD86 and CD206 on M1 and M2 macrophages for mouse normal skin is shown in Fig. S4, and for

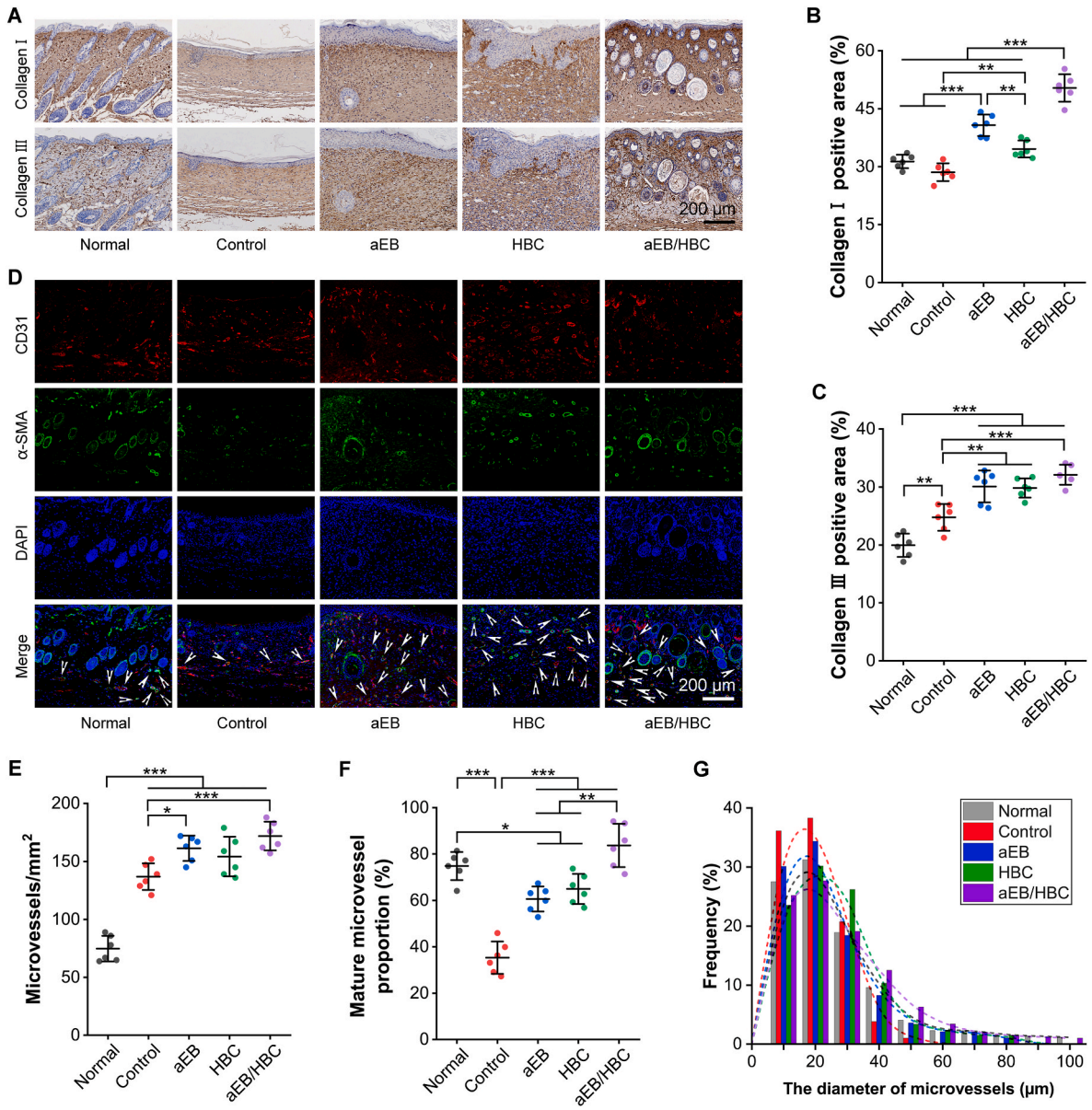

Fig. 7. Immunohistochemical and immunofluorescence staining of tissue healing in diabetic wounds on Day 14. (A) Representative type I and type III collagen immunohistochemical staining of granulation tissues for the four groups and normal skin control. (B, C) Quantification of the positive areas of type I (B) and type III collagen (C) ($n = 6$). (D) Representative immunofluorescence double staining of CD31 and α-SMA for microvessels in granulation tissues. Mature microvessels were positive for both CD31 and α-SMA (white arrows). (E) Quantification of the number of microvessels ($n = 6$). (F) Mature microvessel proportion assay ($n = 6$). (G) Microvessel diameter distribution. $^{*}p < 0.05$, $^{**}p < 0.01$ and $^{***}p < 0.001$.

wounds, it is shown in Fig. 8A. The quantification of M1 and M2 macrophage numbers is shown in Fig. 8B and C, and the ratio of M2/M1 macrophages is shown in Fig. 8D. The normal skin had many CD206-positive M2 macrophages and a small number of CD86-positive M1 macrophages (Fig. S4). At different times, the HBC group had the greatest number of infiltrated M1 macrophages ($CD86^{+}$), and the control group presented the second greatest number (Fig. 8A and B). From Day 3 to Day14, the M1 macrophage numbers continually decreased with time for the control group and the HBC group. On Days 3 and 14, the aEB/HBC group had similar M1 macrophage numbers to the aEB group ($p = 0.411$ and 0.202). On Day 7, the aEB/HBC group had a greater number of M1 macrophages than the aEB group ($p = 0.002$). As shown in Fig. 8A and C, on Day 3, the HBC group had a greater number of M2 macrophages (CD206+) than the aEB group ($p = 0.001$). The aEB/HBC group had a similar number of M2 macrophages to the control group ($p = 0.313$). The aEB/HBC group and the control group had more M2 macrophages than the aEB group and the HBC group (all $p < 0.001$). On day 7, the aEB, HBC, and aEB/HBC groups had similar numbers of M2 macrophages, while the control group had the smallest number of M2 macrophages. On Day 14, the HBC group had the most M2 macrophages, while the control group had the fewest. The number of M2 macrophages in the aEB/HBC group was similar to that in the aEB group. Fig. 8D reveals that the aEB/HBC group had the highest M2/M1 macrophage ratio, while the HBC group had the lowest M2/M1 macrophage ratio at the wound site on Day 3. On Days 7 and 14, the aEB group had the highest M2/M1 macrophage ratio, and the aEB/HBC group had the second highest, but the control group had the lowest M2/M1 macrophage ratio. These results demonstrated that the HBC hydrogels promote M1 macrophage infiltration in the early inflammatory phase, but the aEB/HBC composite hydrogels continually induce M2 macrophage reactions.

Fig. 8E shows that the mRNA ratios of ARG1/TNF-α (M2/M1

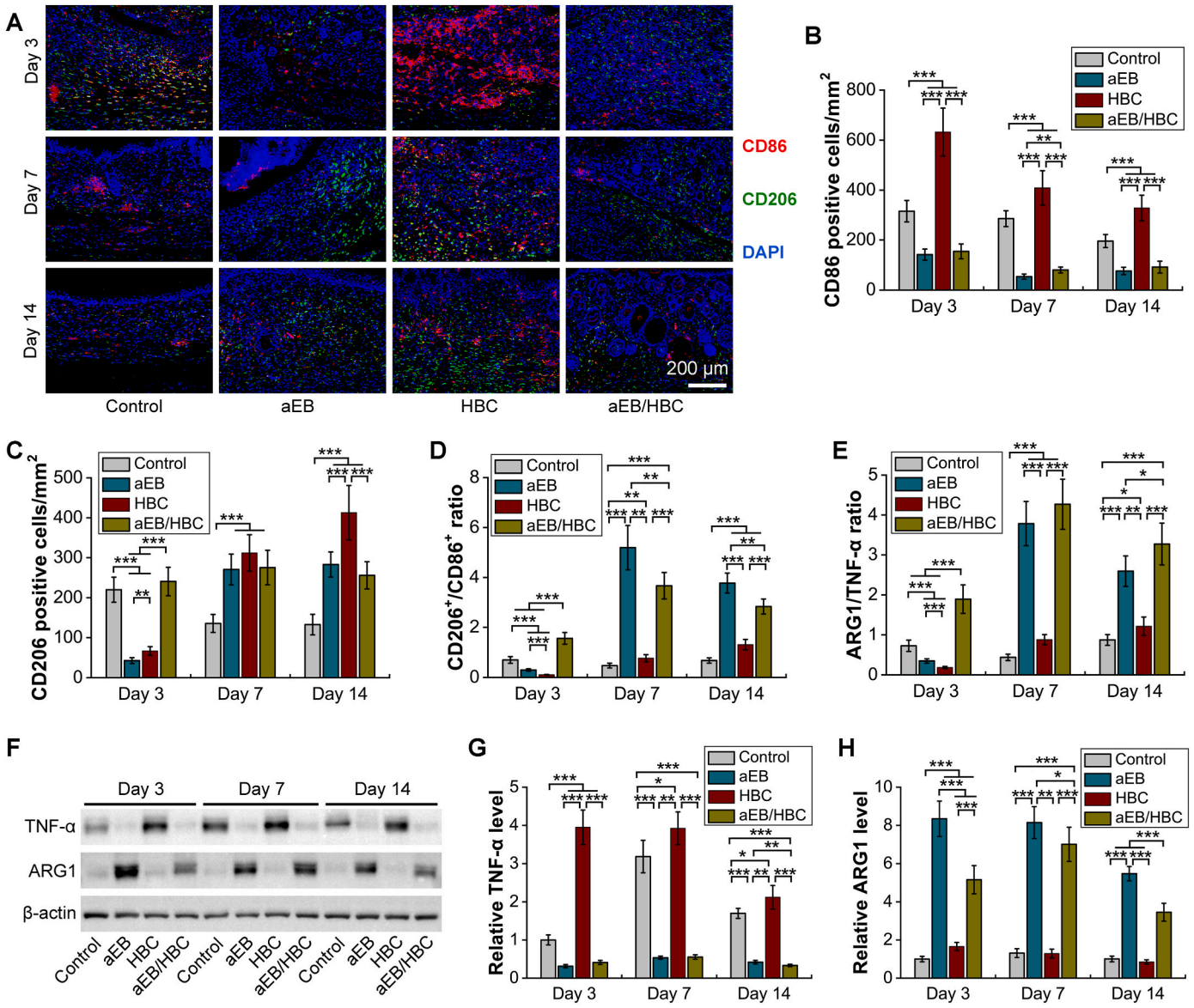

Fig. 8. The immune phenotype and polarization of macrophages at different times during diabetic wound healing. (A) Representative immunofluorescence double staining with CD86 (M1) and CD206 (M2), and nuclei were stained by DAPI. (B) M1 macrophage numbers in the blank control, acellular EB, HBC hydrogel and aEB/HBC composite hydrogel groups ($n = 6$). (C) M2 macrophage number comparisons (n = 6). (D) The M2/M1 ratio (CD206+ cells/CD86+ cells) ($n = 6$). (E) Relative ARG1 and TNF-α mRNA ratios in the four groups ($n = 6$). (F) Representative western blot of TNF-α, ARG1 and β-actin on Days 3, 7 and 14. (G, H) Quantitative analysis of the relative protein band density of TNF-α (G) and ARG1 (H). $^{*}p < 0.05$, $^{**}p < 0.01$ and $^{***}p < 0.001$.

polarization) increased with time for the HBC group. On Day 3, the aEB/HBC group had the highest ARG1/TNF-α mRNA ratio, while the HBC group had the lowest ratio. On Days 7 and 14, the aEB/HBC group presented the highest ARG1/TNF-α mRNA ratio, the aEB group presented the second highest, and the control group had the lowest ARG1/TNF-α mRNA ratio. Fig. 8F and G shows the western blot analysis of TNF-α levels. The TNF-α levels increased from Day 3 to Day 7 but decreased from Day 7 to Day 14 for the control, aEB and aEB/HBC groups. For the HBC group, the TNF-α levels on Day 7 were similar to those on Day 3 but decreased on Day 14. The HBC group had the highest TNF-α levels, and the control group had the second highest on Days 3, 7 and 14. The aEB/HBC group had similar TNF-α levels as the aEB group on Days 3 and 7 ($p = 0.055$ and $p = 0.556$) but had lower TNF-α levels than the aEB group on Day 14 ($p = 0.004$). Fig. 8F and H shows that the ARG1 levels continually decreased in the HBC group but increased from Day 3 to Day 7 and decreased from Day 7 to Day 14 in the control and aEB/HBC groups. The ARG1 levels of the aEB group on Day 7 were similar to those on Day 3 but decreased on Day 14. The aEB group exhibited the highest and the aEB/HBC group exhibited the second highest ARG1 levels at different times. On Day 3, the HBC group had higher ARG1 levels than the control group ($p < 0.001$). On Days 7 and 14, the HBC group had similar ARG1 levels to the control group ($p = 0.872$ and $p = 0.068$). The results indicated that both aEBs and aEB/HBC composite hydrogels upregulated M2-related mRNA and protein expression and downregulated M1-related mRNA and protein expression.

For natural biomaterials based on acellular ECM scaffolds, the matrix material itself and degradation products after *in vivo* implantation induce tissue resident macrophages or bone marrow monocyte-derived macrophages to transform into M2 cells [69]. The three-phase natural wound healing process takes place at approximately 72 h for the inflammatory phase, from Day 4 to Day 21 for the proliferative phase, and from 3 weeks to more than 1 year for the remodeling phase [19]. Normal acute wounds progress to the inflammatory state in a timely manner. In

the brief inflammatory phase, macrophages play proinflammatory roles, and the major macrophage phenotype in this phase is the classically activated M1 phenotype. In the proliferative phase, macrophages support healing and stimulate fibroblasts, keratinocytes and endothelial cells to produce ECM, supporting epithelialization and neovascularization. The primary phenotype of macrophages in this phase is the alternatively activated M2 phenotype [70]. These cells generate anti-inflammatory cytokines and play key roles in ECM formation and angiogenesis [71,72]. The predominant macrophage phenotype switches from the M1 proinflammatory phenotype during the inflammatory phase to the M2 healing phenotype during the proliferative phase. During the initial phases of typical wound healing, approximately 85 % of macrophages present in the wound exhibit the M1 pro-inflammatory phenotype, which subsequently transitions to approximately 80 %–85 % anti-inflammatory M2 macrophages between days 5 and 7 [73]. An increased blood glucose level exerts a substantial impact on the immune system, potentially resulting in modifications to the quantity and phenotype of macrophages associated with the wound. The wound-derived macrophages in diabetic mice exhibited an absence of phenotypic transition towards the M2 phenotype. This imbalance in macrophage phenotypes results in a prolonged state of inflammation within the diabetic wound, thereby impeding the pro-healing functions of endothelial cells, keratinocytes, and fibroblasts. The impaired shift of macrophages from M1 to M2 phenotypes in diabetic wounds leads to the accumulation of inflammatory M1 macrophages [74]. Nevertheless, recent studies have shown that M1 and M2 macrophages play different but equally important roles in accelerating wound healing [75]. The transition of M0 to M2 macrophages is not always the solution to accelerate the diabetic wound healing. It is important to maintain a delicate balance between macrophage phenotypes during different phases of wound healing. Macrophage phenotype changes during wound healing from a pro-inflammatory (M1) profile in early stages to a more pro-healing (M2) profile in later stages. Activated macrophages with M1 phenotype provided on day 1 after injury (non-chronic wound) are shown to promote wound healing in a study [76]. Conversely, a diabetic mouse model that administered ex-vivo-activated murine macrophages with IL-4 or IL-10 during the early inflammatory phase after wounding showed impaired skin healing and delayed re-epithelialization [77]. Conditioned media from M1 macrophages promoted epidermal differentiation and keratinization [78]. Chronic wounds exhibit delayed healing due to the prolongation of the inflammatory state [79]. Macrophages also affect fibroblast responses and fibroblast-associated phenotypic transformation to myofibroblasts, which control scar tissue formation [80]. A prolonged inflammatory phase can delay the phenotypic transformation of macrophages and lead to fibrotic wound healing [81]. Hydrogel dressings currently available target only one phase of diabetic wound healing.

The use of hydrogels in biomaterial-based immunomodulation has recently attracted considerable research interest due to their hydrophilic polymer chains, which can replenish wound moisture. Bioactive molecules and cells can be combined with hydrogels to regenerate and repair tissue in a unique way [82]. Collagen/hyaluronan-based hydrogels developed by Hauk and colleagues were found to promote M2 macrophage polarization and suppress M1 macrophage activation in diabetic wounds [83]. Mei and colleagues have recently developed an injectable photocrosslinking silk hydrogel treatment for diabetic wounds, and the hydrogel system improved diabetic wound healing via spatiotemporal immunomodulation [84]. Xiong and colleagues present a whole-course-repair system exert pro-healing effects throughout the inflammation and proliferation stages of diabetic wound healing [85]. The results of the present study indicated that the HBC hydrogels promote the infiltration of M1 macrophages in the inflammatory phase of wound healing. In the proliferative phase, the HBC hydrogels also increased the infiltration of M2 macrophages. However, M1 macrophage hyperplasia and an inappropriate M2/M1 ratio induced epithelial hyperplasia and fibrous scar hyperplasia in the wound site. A mixture of crosslinked bioactive proteins in the decellularized ECM has demonstrated immunomodulatory properties, guiding cell migration, proliferation, and differentiation [22]. aEBs inhibit M1 macrophages in the inflammatory and proliferative phases and increase M2 macrophages in the proliferative phase. Nevertheless, the aEBs lacked timely epidermal healing. The aEB/HBC composite hydrogels could both inhibit M1 macrophages and promote M2 macrophages in the inflammatory and proliferative phases as the HBC hydrogels contain bioactive cytokines and molecules from aEBs. As a result, the aEB/HBC composite hydrogels induced proper M2 macrophage polarization around the wound site, playing an important role in the accelerated wound healing process.

4. Conclusions

In summary, aEB/HBC composite hydrogels were successfully prepared and exhibited reversible temperature-sensitive phase transition behavior. The *in vitro* antimicrobial activity of the aEB/HBC composite hydrogels was excellent. The novel findings of this study are that aEB/HBC composite hydrogels induced M0-to-M2 polarization but not M1-to-M2 macrophage repolarization in culture. The most significant findings of this study are that Full-thickness diabetic wounds treated with the aEB/HBC composite hydrogels exhibited early wound closure, increased collagen deposition, increased M2/M1 macrophage ratios and increased levels of M2 macrophage-related protein expression compared to those treated with the PBS control, aEBs or HBC hydrogels. Moreover, accessory structures in the skin increased in the aEB/HBC composite hydrogel group over time. These results suggest that wound healing in the aEB/HBC composite hydrogel group is both functional and structural. Therefore, the aEB/HBC composite hydrogel is a promising therapeutic agent for accelerating diabetic wound healing. Based on the findings of this study, human derived embryonic stem cell or induced pluripotent stem cell derived aEBs can be used to promote diabetic wound healing in combination with HBC hydrogels for clinical translation in the future.

CRediT authorship contribution statement

Yue Zhang: Project administration, Writing – original draft. **Zheng-Hong Chen:** Data curation, Investigation. **Kun Zhao:** Supervision. **Yu-Dong Mu:** Visualization. **Kun-Long Li:** Validation. **Zhi-Min Yuan:** Investigation. **Zhi-Gang Liu:** Software. **Le Han:** Writing – review & editing. **Wei-Dong Lü:** Funding acquisition, Project administration, Writing – original draft.

Declaration of competing interest

The authors declare that they have no known competing financial interests or personal relationships that could have appeared to influence the work reported in this paper.

Data availability

Data will be made available on request.

Acknowledgements

This research was supported by the Natural Science Basic Research Program of Shaanxi (Program No. 2024JC-YBMS-149 and 2023-JC-QN-0886), Beijing Science and Technology Innovation Medical Development Foundation (No. KC2023-JX-0186-PM018), and Incubation Project for the National Natural Science Foundation of Tumor Hospital of Shaanxi Province (No. SC23B02, SC221107, and SC211710). We thank Shaanxi Provincial Cancer Hospital Translational Medicine Center for the technical and equipment support.

Appendix A. Supplementary data

Supplementary data to this article can be found online at https://doi.org/10.1016/j.mtbio.2024.100975.

References

[1] M. Olsson, K. Jarbrink, U. Divakar, R. Bajpai, Z. Upton, A. Schmidtchen, J. Car, The humanistic and economic burden of chronic wounds: a systematic review, Wound Repair Regen. 27 (1) (2019) 114–125.

[2] V. Falanga, R.R. Isseroff, A.M. Soulika, M. Romanelli, D. Margolis, S. Kapp, M. Granick, K. Harding, Chronic wounds, Nat. Rev. Dis. Prim. 8 (1) (2022) 50.

[3] H.E. desJardins-Park, G.C. Gurtner, D.C. Wan, M.T. Longaker, From chronic wounds to scarring: the growing health Care burden of under- and over-healing wounds, Adv. Wound Care 11 (9) (2022) 496–510.

[4] S.R. Goldberg, R.F. Diegelmann, What makes wounds chronic, Surg. Clin. 100 (4) (2020) 681–693.

[5] Y. Xiong, Q. Feng, L. Lu, X. Qiu, S. Knoedler, A.C. Panayi, D. Jiang, Y. Rinkevich, Z. Lin, B. Mi, G. Liu, Y. Zhao, Metal-organic frameworks and their composites for chronic wound healing: from bench to bedside, Adv. Mater. (2023) e2302587.

[6] E. Antmen, N.E. Vrana, V. Hasirci, The role of biomaterials and scaffolds in immune responses in regenerative medicine: macrophage phenotype modulation by biomaterial properties and scaffold architectures, Biomater. Sci. 9 (24) (2021) 8090–8110.

[7] P.J. Murray, T.A. Wynn, Protective and pathogenic functions of macrophage subsets, Nat. Rev. Immunol. 11 (11) (2011) 723–737.

[8] Z. Liu, Y. Gu, S. Chakarov, C. Bleriot, I. Kwok, X. Chen, A. Shin, W. Huang, R. J. Dress, C.A. Dutertre, A. Schlitzer, J. Chen, L.G. Ng, H. Wang, Z. Liu, B. Su, F. Ginhoux, Fate mapping via ms4a3-expression history traces monocyte-derived cells, Cell 178 (6) (2019) 1509–1525, e19.

[9] Y. Yang, J. Hou, J. Liu, S. Bhushan, G. Wu, The origins of resident macrophages in mammary gland influence the tumorigenesis of breast cancer, Int. Immunopharm. 110 (2022) 109047.

[10] C. Yunna, H. Mengru, W. Lei, C. Weidong, Macrophage M1/M2 polarization, Eur. J. Pharmacol. 877 (2020) 173090.

[11] C. Savitri, J.W. Kwon, V. Drobyshava, S.S. Ha, K. Park, M2 macrophage-derived concentrated conditioned media significantly improves skin wound healing, Tissue Eng. Regen. Med. 19 (3) (2022) 617–628.

[12] W. Liu, R. Gao, C. Yang, Z. Feng, W. Ou-Yang, X. Pan, P. Huang, C. Zhang, D. Kong, W. Wang, ECM-mimetic immunomodulatory hydrogel for methicillin-resistant Staphylococcus aureus-infected chronic skin wound healing, Sci. Adv. 8 (27) (2022) eabn7006.

[13] K. Xu, S. Deng, Y. Zhu, W. Yang, W. Chen, L. Huang, C. Zhang, M. Li, L. Ao, Y. Jiang, X. Wang, Q. Zhang, Platelet rich plasma loaded multifunctional hydrogel accelerates diabetic wound healing via regulating the continuously abnormal microenvironments, Adv. Healthcare Mater. (2023) e2301370.

[14] Z. Zhou, T. Deng, M. Tao, L. Lin, L. Sun, X. Song, D. Gao, J. Li, Z. Wang, X. Wang, J. Li, Z. Jiang, L. Luo, L. Yang, M. Wu, Snail-inspired AFG/GelMA hydrogel accelerates diabetic wound healing via inflammatory cytokines suppression and macrophage polarization, Biomaterials 299 (2023) 122141.

[15] W. Peng, D. Li, K. Dai, Y. Wang, P. Song, H. Li, P. Tang, Z. Zhang, Z. Li, Y. Zhou, C. Zhou, Recent progress of collagen, chitosan, alginate and other hydrogels in skin repair and wound dressing applications, Int. J. Biol. Macromol. 208 (2022) 400–408.

[16] L. Su, Y. Jia, L. Fu, K. Guo, S. Xie, The emerging progress on wound dressings and their application in clinic wound management, Heliyon 9 (12) (2023) e22520.

[17] P. Varela, S. Sartori, R. Viebahn, J. Salber, G. Ciardelli, Macrophage immunomodulation: an indispensable tool to evaluate the performance of wound dressing biomaterials, J. Appl. Biomater. Funct. Mater. 17 (1) (2019) 2280800019830355.

[18] J. Li, X. Jiang, H. Li, M. Gelinsky, Z. Gu, Tailoring materials for modulation of macrophage fate, Adv. Mater. 33 (12) (2021) e2004172.

[19] A.B. Sousa, A.P. Aguas, M.A. Barbosa, J.N. Barbosa, Immunomodulatory biomaterial-based wound dressings advance the healing of chronic wounds via regulating macrophage behavior, Regen. Biomater. 9 (2022) rbac065.

[20] W. Cao, S. Peng, Y. Yao, J. Xie, S. Li, C. Tu, C. Gao, A nanofibrous membrane loaded with doxycycline and printed with conductive hydrogel strips promotes diabetic wound healing in vivo, Acta Biomater. 152 (2022) 60–73.

[21] G. Theocharidis, H. Yuk, H. Roh, L. Wang, I. Mezghani, J. Wu, A. Kafanas, M. Contreras, B. Sumpio, Z. Li, E. Wang, L. Chen, C.F. Guo, N. Jayaswal, X. L. Katopodi, N. Kalavros, C.S. Nabzdyk, I.S. Vlachos, A. Veves, X. Zhao, A strain-programmed patch for the healing of diabetic wounds, Nat. Biomed. Eng. 6 (10) (2022) 1118–1133.

[22] P. Luo, R. Huang, Y. Wu, X. Liu, Z. Shan, L. Gong, S. Deng, H. Liu, J. Fang, S. Wu, X. Wu, Q. Liu, Z. Chen, K.W.K. Yeung, W. Qiao, S. Chen, Z. Chen, Tailoring the multiscale mechanics of tunable decellularized extracellular matrix (dECM) for wound healing through immunomodulation, Bioact. Mater. 28 (2023) 95–111.

[23] H. Wang, R. Huang, L. Bai, Y. Cai, M. Lei, C. Bao, S. Lin, S. Ji, C. Liu, X. Qu, Extracellular matrix-mimetic immunomodulatory hydrogel for accelerating wound healing, Adv. Healthcare Mater. (2023) e2301264.

[24] Y. Xiong, B.B. Mi, Z. Lin, Y.Q. Hu, L. Yu, K.K. Zha, A.C. Panayi, T. Yu, L. Chen, Z. P. Liu, A. Patel, Q. Feng, S.H. Zhou, G.H. Liu, The role of the immune microenvironment in bone, cartilage, and soft tissue regeneration: from mechanism to therapeutic opportunity, Mil Med. Res. 9 (1) (2022) 65.

[25] A. Biswas, R. Hutchins, Embryonic stem cells, Stem Cell. Dev. 16 (2) (2007) 213–222.

[26] A. Barzegari, V. Gueguen, Y. Omidi, A. Ostadrahimi, M. Nouri, G. Pavon-Djavid, The role of Hippo signaling pathway and mechanotransduction in tuning embryoid body formation and differentiation, J. Cell. Physiol. 235 (6) (2020) 5072–5083.

[27] M. Brown, J. Li, C. Moraes, M. Tabrizian, N.Y.K. Li-Jessen, Decellularized extracellular matrix: new promising and challenging biomaterials for regenerative medicine, Biomaterials 289 (2022) 121786.

[28] X. Zhang, X. Chen, H. Hong, R. Hu, J. Liu, C. Liu, Decellularized extracellular matrix scaffolds: recent trends and emerging strategies in tissue engineering, Bioact. Mater. 10 (2022) 15–31.

[29] A.D. McInnes, M.A.J. Moser, X. Chen, Preparation and use of decellularized extracellular matrix for tissue engineering, J. Funct. Biomater. 13 (4) (2022) 240.

[30] Y. Yan, L.M. Martin, D.B. Bosco, J.L. Bundy, R.S. Nowakowski, Q.X. Sang, Y. Li, Differential effects of acellular embryonic matrices on pluripotent stem cell expansion and neural differentiation, Biomaterials 73 (2015) 231–242.

[31] S. Sart, R. Jeske, X. Chen, T. Ma, Y. Li, Engineering stem cell-derived extracellular matrices: decellularization, characterization, and biological function, Tissue Eng., Part B 26 (5) (2020) 402–422.

[32] S.K. Goh, P. Olsen, I. Banerjee, Extracellular matrix aggregates from differentiating embryoid bodies as a scaffold to support ESC proliferation and differentiation, PLoS One 8 (4) (2013) e61856.

[33] S. Sart, T. Ma, Y. Li, Extracellular matrices decellularized from embryonic stem cells maintained their structure and signaling specificity, Tissue Eng. 20 (1–2) (2014) 54–66.

[34] A. Revete, A. Aparicio, B.A. Cisterna, J. Revete, L. Luis, E. Ibarra, E.A. Segura Gonzalez, J. Molino, D. Reginensi, Advancements in the use of hydrogels for regenerative medicine: properties and biomedical applications, Int. J. Biomater. 2022 (2022) 3606765.

[35] R. Dimatteo, N.J. Darling, T. Segura, In situ forming injectable hydrogels for drug delivery and wound repair, Adv. Drug Deliv. Rev. 127 (2018) 167–184.

[36] M. Kharaziha, A. Baidya, N. Annabi, Rational design of immunomodulatory hydrogels for chronic wound healing, Adv. Mater. 33 (39) (2021) e2100176.

[37] N. Annabi, D. Rana, E. Shirzaei Sani, R. Portillo-Lara, J.L. Gifford, M.M. Fares, S. M. Mithieux, A.S. Weiss, Engineering a sprayable and elastic hydrogel adhesive with antimicrobial properties for wound healing, Biomaterials 139 (2017) 229–243.

[38] E. Zhang, Q. Guo, F. Ji, X. Tian, J. Cui, Y. Song, H. Sun, J. Li, F. Yao, Thermoresponsive polysaccharide-based composite hydrogel with antibacterial and healing-promoting activities for preventing recurrent adhesion after adhesiolysis, Acta Biomater. 74 (2018) 439–453.

[39] G. Xia, Y. Liu, M. Tian, P. Gao, Z. Bao, X. Bai, X. Yu, X. Lang, S. Hu, X. Chen, Nanoparticles/thermosensitive hydrogel reinforced with chitin whiskers as a wound dressing for treating chronic wounds, J. Mater. Chem. B 5 (17) (2017) 3172–3185.

[40] M.P. Tian, A.D. Zhang, Y.X. Yao, X.G. Chen, Y. Liu, Mussel-inspired adhesive and polypeptide-based antibacterial thermo-sensitive hydroxybutyl chitosan hydrogel as BMSCs 3D culture matrix for wound healing, Carbohydr. Polym. 261 (2021) 117878.

[41] C.Z. Wei, C.L. Hou, Q.S. Gu, L.X. Jiang, B. Zhu, A.L. Sheng, A thermosensitive chitosan-based hydrogel barrier for post-operative adhesions' prevention, Biomaterials 30 (29) (2009) 5534–5540.

[42] T. Lim, Q. Tang, Z. Zhu, X. Wei, C. Zhang, Sustained release of human platelet lysate growth factors by thermosensitive hydroxybutyl chitosan hydrogel promotes skin wound healing in rats, J. Biomed. Mater. Res. 108 (10) (2020) 2111–2122.

[43] X. Dong, F. Yao, L. Jiang, L. Liang, H. Sun, S. He, M. Shi, Z. Guo, Q. Yu, M. Yao, P. Che, H. Zhang, J. Li, Facile preparation of a thermosensitive and antibiofouling physically crosslinked hydrogel/powder for wound healing, J. Mater. Chem. B 10 (13) (2022) 2215–2229.

[44] H.E. Rozan, G. Wu, Z. Zhou, Q. Li, M. Sharaf, X. Chen, The complex hydrogel based on diatom biosilica and hydroxybutyl chitosan for wound healing, Colloids Surf. B Biointerfaces 216 (2022) 112523.

[45] Y. Xiong, L. Chen, P. Liu, T. Yu, C. Lin, C. Yan, Y. Hu, W. Zhou, Y. Sun, A.C. Panayi, F. Cao, H. Xue, L. Hu, Z. Lin, X. Xie, X. Xiao, Q. Feng, B. Mi, G. Liu, All-in-One: multifunctional hydrogel accelerates oxidative diabetic wound healing through timed-release of exosome and fibroblast growth factor, Small 18 (1) (2022) e2104229.

[46] W.D. Lü, L. Cai, J.D. Zhang, G.Y. Lei, Z.G. Liu, X.W. Zhang, J.R. Lu, Acellular embryoid bodies in mice: preparation and effect of promoting differentiation of Lewis lung carcinoma cells, Chin. J. Tissue Eng. Res. 20 (20) (2016) 2972–2978.

[47] W.D. Lu, L. Zhang, C.L. Wu, Z.G. Liu, G.Y. Lei, J. Liu, W. Gao, Y.R. Hu, Development of an acellular tumor extracellular matrix as a three-dimensional scaffold for tumor engineering, PLoS One 9 (7) (2014) e103672.

[48] W.D. Lu, R.F. Sun, Y.R. Hu, J.R. Lu, L. Gu, Z.G. Liu, G.Y. Lei, Z. Qiang, L. Cai, Photooxidatively crosslinked acellular tumor extracellular matrices as potential tumor engineering scaffolds, Acta Biomater. 71 (2018) 460–473.

[49] C.B. Anders, T.M.W. Lawton, H.L. Smith, J. Garret, M.M. Doucette, M.C. B. Ammons, Use of integrated metabolomics, transcriptomics, and signal protein profile to characterize the effector function and associated metabotype of polarized macrophage phenotypes, J. Leukoc. Biol. 111 (3) (2022) 667–693.

[50] W.D. Lu, Y.Z. Liu, Z.G. Liu, C.L. Wu, G.Y. Lei, X. Zhang, W. Gao, Y.R. Hu, Effect of lyophilization technique and gamma-ray sterilization on structural, mechanical and biological properties of acellular tumor extracellular matrix scaffolds, J. Biomater. Tiss Eng. 6 (3) (2016) 224–231.

[51] W.D. Lu, Y.Z. Liu, Y.Q. Yang, Z.G. Liu, K. Zhao, J.R. Lu, G.Y. Lei, Y.Y. Wang, L. Cai, R.F. Sun, Effect of naturally derived surgical hemostatic materials on the

proliferation of A549 human lung adenocarcinoma cells, Mater. Today Bio. 14 (2022) 100233.
[52] R.M. Wang, T.D. Johnson, J. He, Z. Rong, M. Wong, V. Nigam, A. Behfar, Y. Xu, K. L. Christman, Humanized mouse model for assessing the human immune response to xenogeneic and allogeneic decellularized biomaterials, Biomaterials 129 (2017) 98–110.
[53] H. Chen, Y. Cheng, J. Tian, P. Yang, X. Zhang, Y. Chen, Y. Hu, J. Wu, Dissolved oxygen from microalgae-gel patch promotes chronic wound healing in diabetes, Sci. Adv. 6 (20) (2020) eaba4311.
[54] N.C. Carrejo, A.N. Moore, T.L. Lopez Silva, D.G. Leach, I.C. Li, D.R. Walker, J. D. Hartgerink, Multidomain peptide hydrogel accelerates healing of full-thickness wounds in diabetic mice, ACS Biomater. Sci. Eng. 4 (4) (2018) 1386–1396.
[55] W.D. Lu, M. Zhang, Z.S. Wu, T.H. Hu, Z.J. Xu, W. Liu, Y.R. Hu, The performance of photooxidatively crosslinked acellular bovine jugular vein conduits in the reconstruction of connections between pulmonary arteries and right ventricles, Biomaterials 31 (10) (2010) 2934–2943.
[56] N. Weidner, J.P. Semple, W.R. Welch, J. Folkman, Tumor angiogenesis and metastasis–correlation in invasive breast carcinoma, N. Engl. J. Med. 324 (1) (1991) 1–8.
[57] S. Lecht, C.T. Stabler, A.L. Rylander, R. Chiaverelli, E.S. Schulman, C. Marcinkiewicz, P.I. Lelkes, Enhanced reseeding of decellularized rodent lungs with mouse embryonic stem cells, Biomaterials 35 (10) (2014) 3252–3262.
[58] C. Wang, G. Li, K. Cui, Z. Chai, Z. Huang, Y. Liu, S. Chen, H. Huang, K. Zhang, Z. Han, Y. Li, G. Yu, Z.C. Han, N. Liu, Z. Li, Sulfated glycosaminoglycans in decellularized placenta matrix as critical regulators for cutaneous wound healing, Acta Biomater. 122 (2021) 199–210.
[59] Z. Aliakbar Ahovan, Z. Esmaeili, B.S. Eftekhari, S. Khosravimelal, M. Alehosseini, G. Orive, A. Dolatshahi-Pirouz, N. Pal Singh Chauhan, P.A. Janmey, A. Hashemi, S. C. Kundu, M. Gholipourmalekabadi, Antibacterial smart hydrogels: new hope for infectious wound management, Mater. Today Bio. 17 (2022) 100499.
[60] S. Cheng, H. Wang, X. Pan, C. Zhang, K. Zhang, Z. Chen, W. Dong, A. Xie, X. Qi, Dendritic hydrogels with robust inherent antibacterial properties for promoting bacteria-infected wound healing, ACS Appl. Mater. Interfaces 14 (9) (2022) 11144–11155.
[61] D. Hu, J. Wen, X. Zhao, K. Liu, Y. Zhang, Y. Bu, K. Wang, A wound-friendly antibacterial hyaluronic acid dressing with on-demand removability for infected wound healing, Biomater. Res. 27 (1) (2023) 38.
[62] Y. Yang, X. Zhao, J. Yu, X. Chen, R. Wang, M. Zhang, Q. Zhang, Y. Zhang, S. Wang, Y. Cheng, Bioactive skin-mimicking hydrogel band-aids for diabetic wound healing and infectious skin incision treatment, Bioact. Mater. 6 (11) (2021) 3962–3975.
[63] W. Zhang, S. Xia, T. Weng, M. Yang, J. Shao, M. Zhang, J. Wang, P. Xu, J. Wei, R. Jin, M. Yu, Z. Zhang, C. Han, X. Wang, Antibacterial coaxial hydro-membranes accelerate diabetic wound healing by tuning surface immunomodulatory functions, Mater. Today Bio. 16 (2022) 100395.
[64] S. Chen, A. Saeed, Q. Liu, Q. Jiang, H. Xu, G.G. Xiao, L. Rao, Y. Duo, Macrophages in immunoregulation and therapeutics, Signal Transduct. Targeted Ther. 8 (1) (2023) 207.
[65] J. Van den Bossche, J. Baardman, N.A. Otto, S. van der Velden, A.E. Neele, S. M. van den Berg, R. Luque-Martin, H.J. Chen, M.C. Boshuizen, M. Ahmed, M. A. Hoeksema, A.F. de Vos, M.P. de Winther, Mitochondrial dysfunction prevents repolarization of inflammatory macrophages, Cell Rep. 17 (3) (2016) 684–696.
[66] Y. Xiong, X. Chu, T. Yu, S. Knoedler, A. Schroeter, L. Lu, K. Zha, Z. Lin, D. Jiang, Y. Rinkevich, A.C. Panayi, B. Mi, G. Liu, Y. Zhao, Reactive oxygen species-scavenging nanosystems in the treatment of diabetic wounds, Adv. Healthcare Mater. 12 (25) (2023) e2300779.
[67] G.J. Kotwal, S. Chien, Macrophage differentiation in normal and accelerated wound healing, Results Probl. Cell Differ. 62 (2017) 353–364.
[68] G. Zhang, Z. Zhang, G. Cao, Q. Jin, L. Xu, J. Li, Z. Liu, C. Xu, Y. Le, Y. Fu, J. Ju, B. Li, R. Hou, Engineered dermis loaded with confining forces promotes full-thickness wound healing by enhancing vascularisation and epithelialisation, Acta Biomater. 170 (2023) 464–478.
[69] J. Mao, L. Chen, Z. Cai, S. Qian, Z. Liu, B. Zhao, Y. Zhang, X. Sun, W. Cui, Advanced biomaterials for regulating polarization of macrophages in wound healing, Adv. Funct. Mater. 32 (12) (2022) 2111003.
[70] B. Mahdavian Delavary, W.M. van der Veer, M. van Egmond, F.B. Niessen, R. H. Beelen, Macrophages in skin injury and repair, Immunobiology 216 (7) (2011) 753–762.
[71] K.L. Spiller, R.R. Anfang, K.J. Spiller, J. Ng, K.R. Nakazawa, J.W. Daulton, G. Vunjak-Novakovic, The role of macrophage phenotype in vascularization of tissue engineering scaffolds, Biomaterials 35 (15) (2014) 4477–4488.
[72] P. Krzyszczyk, R. Schloss, A. Palmer, F. Berthiaume, The role of macrophages in acute and chronic wound healing and interventions to promote pro-wound healing phenotypes, Front. Physiol. 9 (2018) 419.
[73] S.M. Aitcheson, F.D. Frentiu, S.E. Hurn, K. Edwards, R.Z. Murray, Skin wound healing: normal macrophage function and macrophage dysfunction in diabetic wounds, Molecules 26 (16) (2021).
[74] M. Sharifiaghdam, E. Shaabani, R. Faridi-Majidi, S.C. De Smedt, K. Braeckmans, J. C. Fraire, Macrophages as a therapeutic target to promote diabetic wound healing, Mol. Ther. 30 (9) (2022) 2891–2908.
[75] K.E. Martin, A.J. Garcia, Macrophage phenotypes in tissue repair and the foreign body response: implications for biomaterial-based regenerative medicine strategies, Acta Biomater. 133 (2021) 4–16.
[76] X.Y. Gu, S.E. Shen, C.F. Huang, Y.N. Liu, A.P. Wang, Effect of activated autologous monocytes/macrophages on wound healing in a rodent model of experimental diabetes, Diabetes Res. Clin. Pract. 102 (1) (2013) 53–59.
[77] N. Jetten, N. Roumans, M.J. Gijbels, A. Romano, M.J. Post, M.P. de Winther, R. R. van der Hulst, S. Xanthoulea, Wound administration of M2-polarized macrophages does not improve murine cutaneous healing responses, PLoS One 9 (7) (2014) e102994.
[78] G. Theocharidis, S. Rahmani, S. Lee, Z. Li, A. Lobao, K. Kounas, X.L. Katopodi, P. Wang, S. Moon, I.S. Vlachos, M. Niewczas, D. Mooney, A. Veves, Murine macrophages or their secretome delivered in alginate dressings enhance impaired wound healing in diabetic mice, Biomaterials 288 (2022) 121692.
[79] R. Zhao, H. Liang, E. Clarke, C. Jackson, M. Xue, Inflammation in chronic wounds, Int. J. Mol. Sci. 17 (12) (2016) 2085.
[80] Z. Li, K.M. Bratlie, Fibroblasts treated with macrophage conditioned medium results in phenotypic shifts and changes in collagen organization, Mater. Sci. Eng., C 122 (2021) 111915.
[81] Z. Zhu, J. Ding, Z. Ma, T. Iwashina, E.E. Tredget, Systemic depletion of macrophages in the subacute phase of wound healing reduces hypertrophic scar formation, Wound Repair Regen. 24 (4) (2016) 644–656.
[82] Y. Xiong, Q. Feng, L. Lu, K. Zha, T. Yu, Z. Lin, Y. Hu, A.C. Panayi, V. Nosrati-Ziahmagi, X. Chu, L. Chen, M.-A. Shahbazi, B. Mi, G. Liu, Immunomodulatory hydrogels: advanced regenerative tools for diabetic foot ulcer, Adv. Funct. Mater. 33 (10) (2023) 2213066.
[83] S. Hauck, P. Zager, N. Halfter, E. Wandel, M. Torregrossa, A. Kakpenova, S. Rother, M. Ordieres, S. Rathel, A. Berg, S. Moller, M. Schnabelrauch, J.C. Simon, V. Hintze, S. Franz, Collagen/hyaluronan based hydrogels releasing sulfated hyaluronan improve dermal wound healing in diabetic mice via reducing inflammatory macrophage activity, Bioact. Mater. 6 (12) (2021) 4342–4359.
[84] J. Mei, J. Zhou, L. Kong, Y. Dai, X. Zhang, W. Song, C. Zhu, An injectable photo-cross-linking silk hydrogel system augments diabetic wound healing in orthopaedic surgery through spatiotemporal immunomodulation, J. Nanobiotechnol. 20 (1) (2022) 232.
[85] Y. Xiong, Z. Lin, P. Bu, T. Yu, Y. Endo, W. Zhou, Y. Sun, F. Cao, G. Dai, Y. Hu, L. Lu, L. Chen, P. Cheng, K. Zha, M.A. Shahbazi, Q. Feng, B. Mi, G. Liu, A whole-course-repair system based on neurogenesis-angiogenesis crosstalk and macrophage reprogramming promotes diabetic wound healing, Adv. Mater. 35 (19) (2023) e2212300.